(1)

(6) METAL-SILICON SCHOTTKY BARRIER INFRARED VIDICON,

(10) J. P. Spratt,
R. F. Schwarz
G. W. Racette

(12) 63 p.

(11) 22 MAR 76

(15) F19628-76-C-0091
ARPA Order-2444

~~Space Sciences Laboratory~~
GENERAL ELECTRIC COMPANY
Space Division
P.O. Box 8555
Philadelphia, Pennsylvania 19101

405025

TABLE OF CONTENTS

LIST OF ILLUSTRATIONS

LIST OF ILLUSTRATIONS

ABSTRACT

A new type of infrared vidicon camera tube has been developed which overcomes many of the objections previously raised against this approach to infrared imaging. This new vidicon employs high beam velocity scanning of a matrix of metal-silicon Schottky barrier diodes. These diodes achieve mid-IR response as a result of internal photoemission over the metal-silicon barrier. Feasibility demonstration experiments have demonstrated good imagery, and have permitted the evaluation of certain key parameters such as the quantum efficiency coefficient (C_1) and resolution element size (A_e). Using these parameters, it can be shown that a 5 μm tube using PtSi/p-type silicon diodes will be capable of 0.2°C Minimum Resolvable Temperature Difference at 500 TV lines resolution. For detection of high temperature (1000°K) point sources, Noise Equivalent Power of 1.3×10^{-11} watts at $A_e = 8 \times 10^{-5}$ cm^2 is predicted. Considering the fact that infrared imagers employing these vidicons will be substantially less expensive (1 to 2 orders of magnitude) than conventional imagers of comparable performance, these performance predictions appear quite attractive.

This research was partially supported by the Defense Advanced Research Projects Agency under ARPA Order No. 2444 and sponsored by Air Force Cambridge Research Labs.

I. INTRODUCTION

Television systems for the visible portion of the spectrum typically use frame time integration to enhance sensitivity before readout. Contrast in this application is typically 20% or better, so that the minimum detectable signal is set, not by fluctuations in the signal or the background, but rather by a fixed noise source such as the input of the preamplifier. If one attempts to apply this technique to the infrared,[1] where low contrast conditions exist because of thermal radiation from the background, several problems arise, viz:

- Detector saturation by background photon flux.
- Non-uniformity in responsivity over the sensing layer will, when operating against a high background, generate a fixed pattern "noise," which while not truly random, limits the ability to detect low level signals conveniently.

To minimize the latter problem, highly uniform sensing layers are needed. Depending upon the thermal resolution required of an infrared camera tube and the spectral range of operation, allowable variations in photoresponse over the sensing layer must be in the range 0.1% to 1.0%.[2] Such stringent uniformity requirements are beyond the capability of present technology in conventional photoconductive or photovoltaic detectors. Doping density, minority carrier lifetime, or semiconductor composition (for compounds) cannot be controlled to this precision. Consequently, images obtained with infrared camera tubes have, in the past, been inferior to those obtained with line scanners which provide no frame time integration, but simply respond to the instantaneous radiation flux incident on them. Recently, however, a novel approach to infrared sensing layers has been suggested.[3, 4, 5] The new sensing layer consists of a matrix of metal-silicon Schottky barrier diodes employing internal photoemission[6] to achieve response at wavelengths longer than the fundamental edge in silicon. Internal photoemissive detectors are largely independent of both minority carrier lifetime and doping density in the semiconductor, and dependent only on the barrier height of the Schottky diode and the electronic properties of the metal. The use of silicon monolithic processing technology permits large arrays of these devices to be fabricated with highly uniform properties. These two characteristics (inherent uniformity and relative ease of fabrication) should permit the high degree of sensing layer uniformity necessary to allow infrared camera

tubes to compete successfully with line scanners at wavelengths out to five microns. This paper describes the experiments conducted to show the feasibility of this new type of camera tube, presents the results obtained in imaging studies, and describes the performance expected for optimized versions of these tubes.

II. DESCRIPTION OF FEASIBILITY EXPERIMENTS

Internal photoemission in metal-silicon Schottky barrier diode structures has long been known to permit the detection of infrared radiation of wavelengths longer than the fundamental absorption edge in silicon. This process, while generally analogous to photoemission into vacuum, has certain features which are unique and have no direct counterpart in the older technology, e.g., photoemission of holes as well as electrons. The former is interesting because it permits the attainment of low barriers (therefore long cutoff wavelengths) with high work function photocathodes, such as the precious metals (Au, Ag, Pt, Pd) on p-type silicon. The polarity of the resultant diode is opposite to that normally used in low beam velocity silicon diode vidicons,[7] and requires the use of a high velocity electron beam scan to bias the diode properly. In this mode of operation,[8] the beam lands on the retina with an energy sufficiently high to dislodge secondary electrons with a yield $\delta > 1$. These secondaries flow to a nearby collector mesh, permitting individual picture elements to charge positively with respect to this collector (and hence to the underlying p-type silicon). Because of the novel nature of both the retinas and the scanning techniques, it was decided to show feasibility in the somewhat less difficult spectral interval of 1-3.5 μm, and later to extend the work into the more useful 3-5 μm region. The initial feasibility demonstration and retina characterization were to be done in a demountable camera tube,[9] with sealed-off tubes to be used once optimum designs could be specified. The essential elements of this demountable tube are shown schematically in Figure 1. These are the electron gun section, beam deflection section, and the retina section. The electron gun section typically contains a thermionic cathode and several other electrodes for forming and modulating an electron beam. The scanning section contains coils (electromagnetic deflection) or plates (electrostatic deflection) for deflecting the beam across the retina surface in a prescribed fashion. The retina section consists of a photosensitive surface which can be charged (by the scanning beam) relative to its opposite (window) side. Light

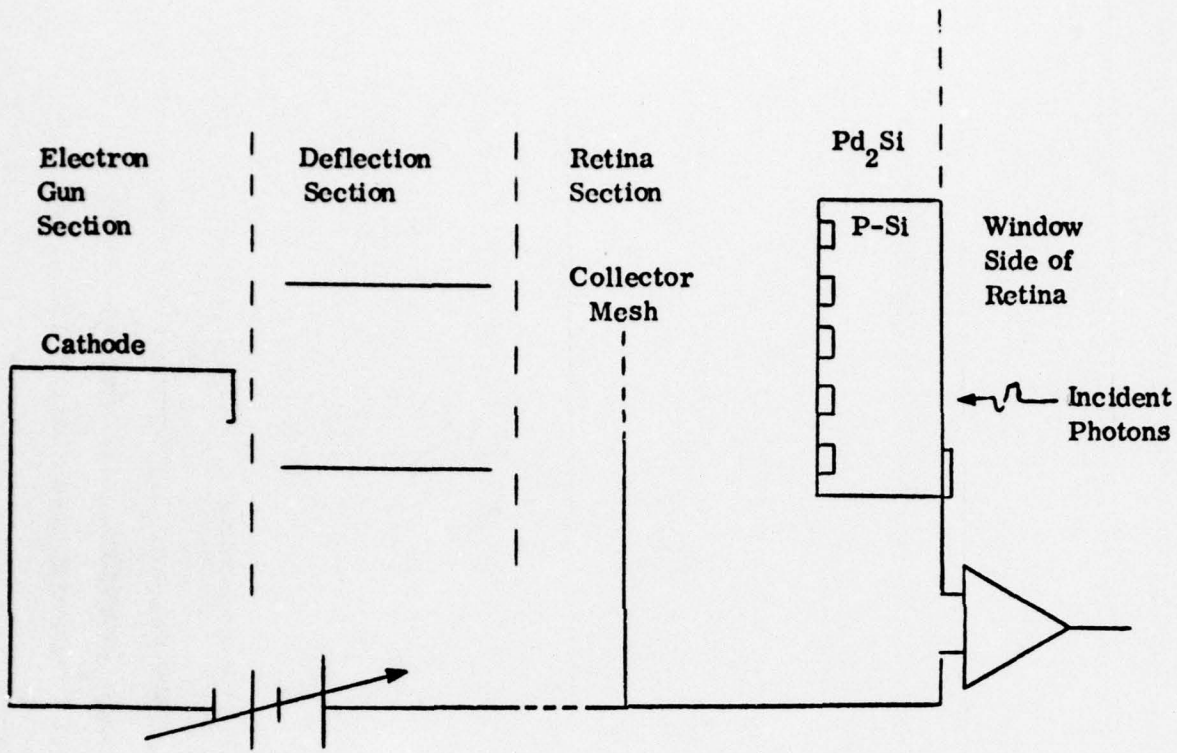

Figure 1. Schematic Diagram of High Beam Velocity Camera Tube.

incident on the window side of the retina will pass through the silicon and discharge the photosensitive surface, necessitating the flow of additional current to recharge the retina during the next scan. This recharging current thus varies in time in a manner which is synchronized with the spatial position of the scanning beam, and hence the spatial pattern of incident light. It constitutes the video signal. This current (I_S) flows for a time t_R, the dwell time of the beam on a given picture element. During this time the potential of this picture element is restored to its equilibrium value. The charge deposited in the process is

$$Q_D = I_S t_R \tag{1}$$

The charged leaked off that picture element by light (Q_L) during the frame time, t_f, is (neglecting dark current)

$$Q_L = I_P t_f = q y i_{ph} t_f \tag{2}$$

where I_P = photocurrent

q = electronic charge

y = quantum efficiency

i_{ph} = photon flux (photons/picture element/second)

In the cyclic state, $Q_D = Q_L$, so that

$$I_S = I_P \frac{t_f}{t_R} = q y \frac{t_f}{t_R} i_{ph} \tag{3}$$

If t_f = 1/30 second, and t_R = 1 μsec, a storage mode gain of $\frac{t_f}{t_R} = 3 \times 10^4$ results to offset the effect of low quantum efficiency inherent in metal-silicon Schottky diodes for radiation of wavelength beyond the fundamental edge of silicon. The equivalent circuit of such an idealized picture element is shown in Figure 2. It can be seen that attainment of the high storage mode gain assumes that the leakage of charge off the capacitor in the absence of light is minimal. To assure that this condition is met it is necessary that the voltage applied to the diode be of the proper polarity (reverse bias), and that the operating temperature be such that the thermally generated leakage current is low. These two requirements and their implications are discussed below.

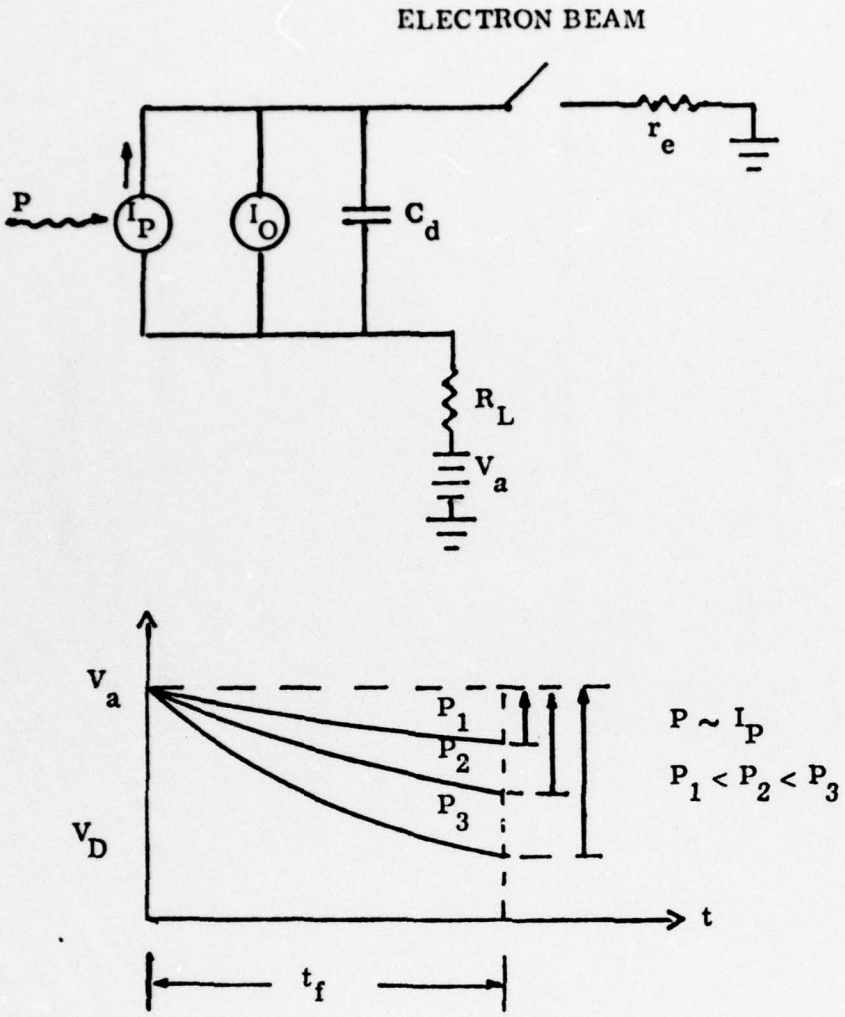

C_d = diode capacitance

I_O = diode reverse leakage

I_P = photocurrent

P = photon flux

r_e = beam resistance

R_L = load resistance

t_f = frame time

V_a = applied voltage

V_D = voltage across C_d

Figure 2. Equivalent Circuit of Picture Element.

A. High Beam Velocity Vidicon Operation

To permit the scanning beam to land on the retina, the common side of any diode mosaic must be biased positively with respect to the cathode. The floating side of the retina will then be charged by the beam to a potential relative to the cathode (and hence to the common side of the diode mosaic) which depends on the velocity with which the beam lands on the floating surface. Conventional camera tubes use electron beams which land at a few volts potential relative to the cathode. If the common side of the diode mosaic is n-type, slow electrons such as these charge the floating side of the retina to a voltage sufficiently negative with respect to the cathode to make it impossible for additional electrons to land. Thus P^+ islands on N material become reverse biased, permitting storage over a full frame time (N^+ islands on P material would become forward biased, and full frame time storage would be impossible). Since the spectral range of both P^+-N and N^+-P mosaics is identical, diode polarity can be selected to permit low beam velocity scanning. Metal-silicon Schottky barrier diodes, however, have an additional constraint placed on them. In order to achieve the desired long wavelength cutoff in the infrared vidicon retina, a metal-silicon system must be chosen which has a low value of barrier height, ϕ_o. This is most easily achieved using high work function metals (such as Pd_2Si) on p-type silicon. Such a choice, however, results in a diode polarity opposite to that normally used in semiconductor diode retinas. Consequently, these mosaics must be scanned with electron beams which land with an energy sufficiently high to dislodge secondary electrons with a yield $\delta > 1$. An individual floating Pd_2Si island will therefore charge positively under a fast beam to a potential, V_{FT}, determined by the collector mesh (mesh stabilized operation) rather than to a potential determined by the cathode, as occurs in low beam velocity scanning. V_{FT} can be determined for the highly idealized case of a homogeneous retina as follows. Assuming that the secondary electrons are Maxwellian one obtains the following equation[10]

$$I_M = \int_{V_{FT}}^{\infty} \frac{di_S}{dV_Z} \, dV_Z = i_S \exp\left(-V_{FT}/\overline{V}\right) \tag{4}$$

where I_M = current of secondary electrons going to the mesh

i_S = secondary electron current generated at the floating target

V_Z = energy component of secondaries normal to plane of target

$\overline{V}$ = average energy of secondaries

The net current supplied by the beam to the floating target is the difference between the primary beam landing and the secondaries going to the mesh, which is

$$I_T = I_B - I_M = I_B - i_S \exp(-V_{FT}/\overline{V})$$

$$= I_B \left[1 - \delta \exp(-V_{FT}/\overline{V})\right] ; \; V_{FT} \geq 0 \tag{5}$$

$$= I_B (1 - \delta) \qquad ; \; V_{FT} < 0 \tag{6}$$

where $i_S = \delta I_B$

I_B = beam current

The floating target will charge to a voltage V_{FT} such that $I_T = 0$, if possible. This will produce

$$V_{FT} = \overline{V} \ln \delta \tag{7}$$

where V_{FT} is positive relative to the mesh. Thus if the common side of the diode mosaic is biased negatively with respect to the mesh, the net voltage between the Pd_2Si island and p-silicon is such that the diode is reverse biased. If we neglect interactions between the Pd_2Si islands and the SiO_2 between these islands, a fast beam scanned across the diode mosaic in raster fashion will charge the metal to V_{FT}. Photocurrents can then discharge the target surface down toward mesh potential during the frame time, so that a signal will be generated between retina and mesh when the beam returns to a given spot during the next scan.

1. Long Wavelength Cutoff Vs. Operating Temperature

The quantum efficiency (y) of the internal photoemission process in metal-silicon Schottky diodes is low, as shown by the following equation[11]

$$y = C_1 \frac{(h\nu - \phi_o)}{h\nu} \; ; \; h\nu \geq \phi_o \tag{8}$$

where C_1 = constant $\approx 0.004/eV$ [4]

ϕ_o = height of metal-silicon barrier in eV

If the barrier height is selected to permit detection out to a cutoff wavelength λ_o ($\lambda_o = 1.24/\phi_o$), the reverse leakage current I_o is affected, since [12]

$$I_o = A^* T^2 \exp(-q\phi_o/kT) \tag{9}$$

where A^* = modified Richardson constant.

The reverse leakage current must be such that the charge leaking off a diode in a frame time is less than the charge on the diode.

$$I_o t_f \leq C_D V_D \tag{10}$$

where C_D = diode capacitance

V_D = voltage across diode

It must also be less than the maximum charge which the beam can deposit in one read time, t_R.

$$I_o t_f \leq I_B (\delta - 1) t_R \tag{11}$$

where $I_B (\delta - 1)$ is the maximum current which the fast beam can deposit on the retina (Cf. equation (5)).

t_R is the time the beam dwells on an individual picture element.

Because of the high specific capacity of diodes, and the limitations on beam current available in camera tubes, equation (11) is a more difficult condition to meet. Using this equation, the temperature to which the retina must be cooled for a given long wavelength cutoff can be determined. For the retina design used herein, operating temperatures $< 110^{\circ}K$ are required.

2. Description of Demountable Tube and Related Equipment

To permit the evaluation of different retina designs and different electron beam scan configurations, a demountable camera tube was designed and built. [9] This tube permits a retina to be scanned on one side with a suitable fast beam of electrons (with

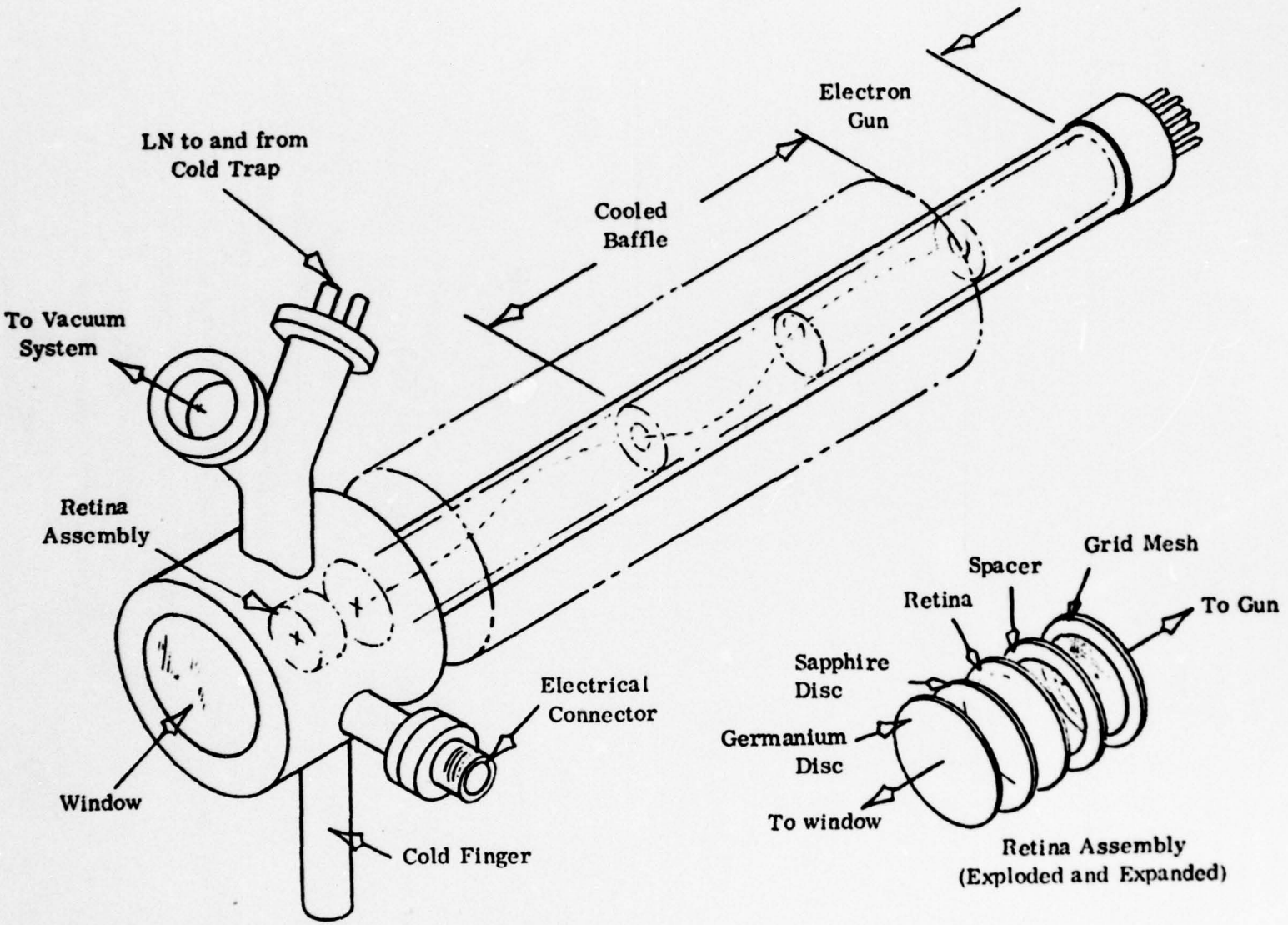

Figure 3. Demountable Camera Tube

provision for collecting secondaries), while the opposite side is being exposed to the optical image. Retina cooling is achieved by radial heat flow to a suitable heat sink. Figure 3 depicts such a demountable camera tube, showing the main features of the system.

B. Schottky Barrier Retinas

1. Retina Design

The particular material system selected for this purpose was palladium on p-type silicon. Palladium forms a stable silicide having a barrier height of 0.35 eV on p-silicon, giving a long wavelength cutoff of 3.54 μm. The mask set used produced a 34 mm diameter array of 8 μm square diodes of 10 μm centers. Cuts were made in this pattern in a 0.5 μm thermal oxide grown on 2-inch wafers of p-type silicon of two different resistivities, 3 ohm-cm and 10 ohm-cm. Palladium of two different thicknesses (500 Å and 5000 Å) was deposited and sintered at 270°C for 5 minutes in 50:50 H_2, N_2. Unreacted palladium was then etched off without removing the Pd_2Si, leaving the desired diode pattern. Ohmic contact to the p-region consisted of an annular ring, 0.125 inch wide and 2 inches O.D. of sintered platinum on the side of the wafer opposite to the diode array. (The forward voltage drop calculated for the Pt-Si contact at 1 μA is 70 meV.) Figure 4 shows a photograph of a finished retina at X1 and X1000.

P-N junction diode array vidicon targets suffer from problems of surface inversion which shorts adjacent diodes. This problem will not bother cooled Schottky diode vidicon targets for two reasons:

(1) There are no means for generating minority carriers in the bulk to re-supply an inverted surface. Thermal generation is minimal, especially at the target operating temperature of 77°K. Optical generation of minority carriers requires photons of $\lambda < 1.1$ μm, which are filtered out by means of a germanium pre-filter.

(2) In the case of adjacent metal islands sitting at different potentials, any minority carriers initially present at the surface will flow to the appropriate island, but the other island cannot serve as a source of additional minority carriers, since its barrier to minority carriers is higher than its barrier to majority carriers.

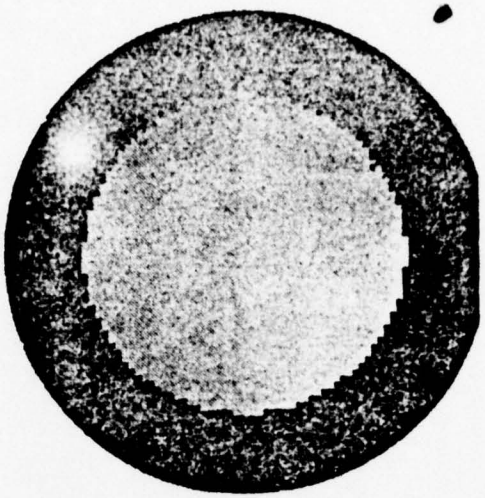

Figure 4. Photographs of Retina at X1 and X1000 Magnification

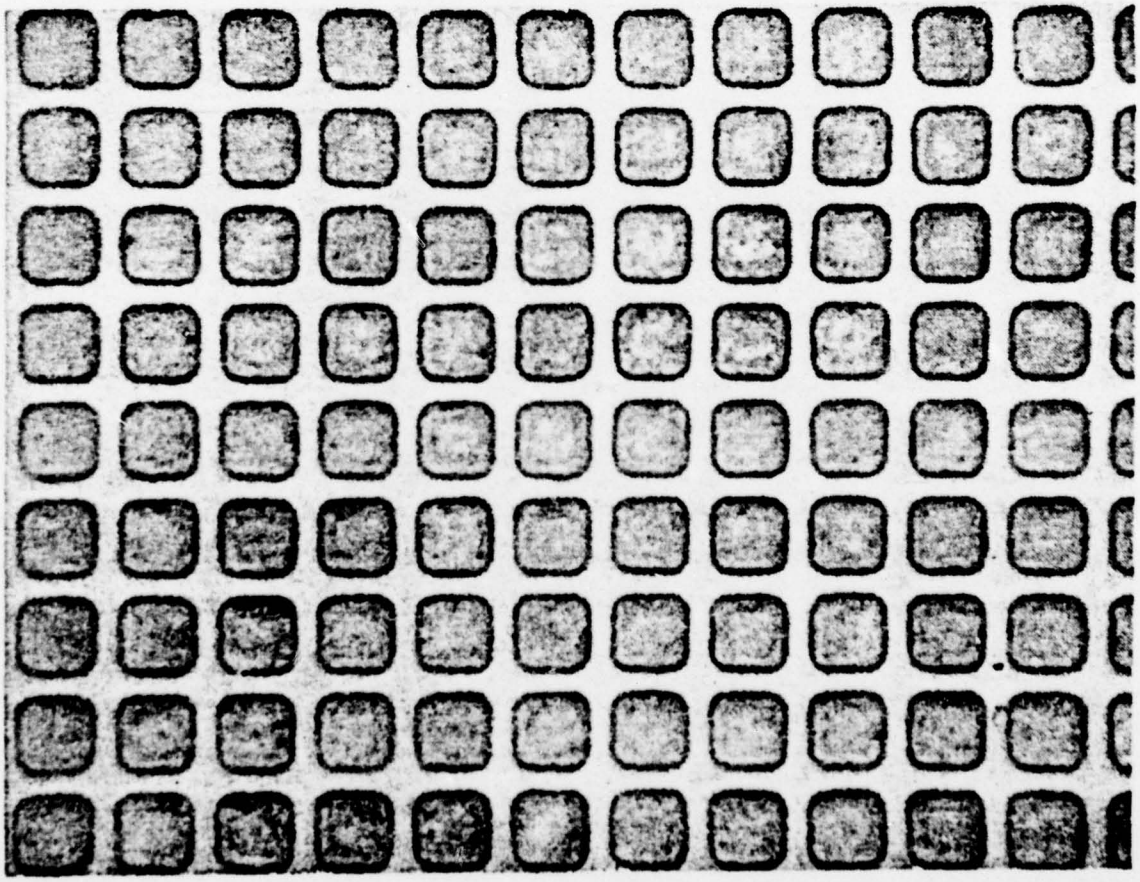

As a result of this freedom from surface inversion, it is found that these retinas do not require a resistive sea. In view of the lack of information on the properties of resistive sea at 77°K, this development is a happy one.

2. Retina Characterization

The single most important task in this whole area of research was that of demonstrating that mosaics of metal-silicon Schottky barrier diodes, fabricated in a conventional integrated circuit facility, could in fact produce images at wavelengths longer than the fundamental edge in silicon. To accomplish this task, several requirements must be imposed on the retina, which can best be described by considering the schematic diagram of a Schottky diode under a fast electron beam (Figure 5).

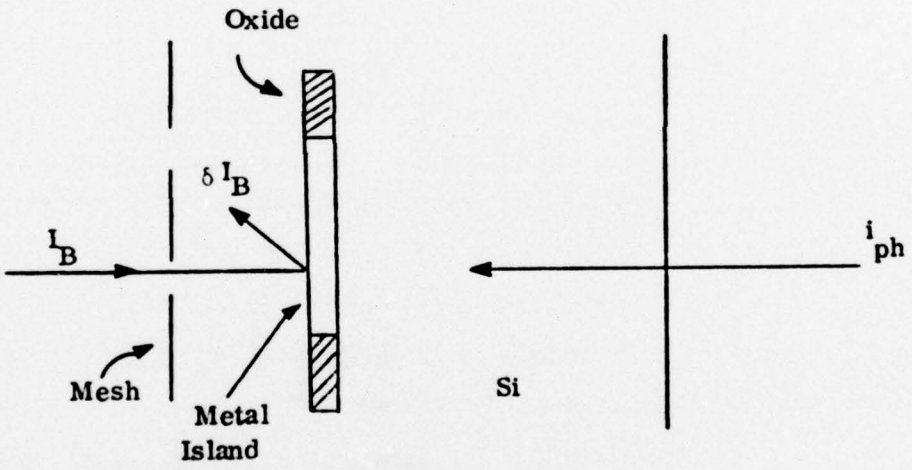

Figure 5. Schematic Diagram of a Schottky Diode under Bombardment by an Electron Beam, I_B

Rewriting equation (5), we see that the target current, I_T, is

$$I_T = -I_B(\delta - 1) + \delta I_B \left(1 - \exp \frac{-V_{TM}}{\overline{V}}\right) \tag{12}$$

The current in the first term on the right of equation (12) is independent of the target to the mesh voltage and behaves like a current generator driving a positive current from mesh to target if δ is greater than 1. The second term on the right of equation (12) represents a current controlled by the target to mesh voltage. This is describable in an equivalent circuit by a voltage dependent resistor, r_b, in parallel with the current generator described by the first term. For a Maxwellian energy distribution, r_b, is by definition

$$1/r_b \equiv \frac{d\left\{\delta I_B \left(1 - \exp \frac{-V_{TM}}{\overline{V}}\right)\right\}}{dV_{TM}}$$

$$= \frac{\delta I_B}{\overline{V}} \exp \frac{-V_{TM}}{\overline{V}} \tag{13}$$

There is also a target to mesh capacitance, C_{TM}, in parallel with r_b and the current generator $I_B(\delta - 1)$. An equivalent circuit for the particular element shown in Figure 5, may thus be described by Figure 6. Here the diode is represented by the parallel combination of a resistance r_D, a capacitance C_{TS}, and a current generator, RP where P is the radiant power incident on the diode, and R is the responsivity of the diode in amps/watt.

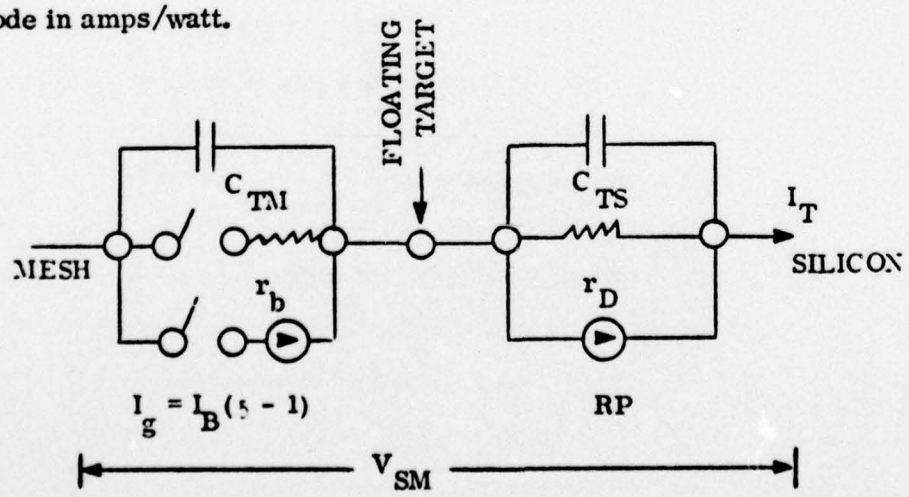

Figure 6. Equivalent Circuit for the Element in Figure 5

The switches in the mesh to target loop are closed during the read time, t_R, when the electron beam is on the diode, and are open during the remainder of the frame time, $t_f - t_R$, which we shall refer to as the storage time.

If in the steady state, no current were flowing out the Si, the current, $(\delta - 1) I_B$, would flow through the resistance r_b, and the voltage V_{TMO} would be determined from (12) as

$$I_B (\delta - 1) = \delta I_B \left[1 - \exp \frac{-V_{TMO}}{\overline{V}} \right]$$

which yields

$$V_{TMO} = \overline{V} \ell n \, \delta \tag{14}$$

In the operation of the tube,

$$0 \lesssim V_{TM} \lesssim V_{TMO} \tag{15}$$

Thus from equations (13), (14), and (15)

$$\frac{\overline{V}}{\delta I_B} \lesssim r_b \lesssim \frac{\overline{V}}{I_B} \tag{16}$$

For δ not too different from unity, r_b does not vary appreciably over the operating range of the tube, and the equivalent circuit of Figure 6 is conceptually quite useful. r_D and C_{TS} will both be voltage dependent, but these dependences are reasonably well understood.

If there are a total of N diodes on the target, the equivalent circuit of the mesh to Si loop is represented by N loops like Figure 6 in parallel, plus a mesh to Si capacitance, C_{MS} also in parallel with these loops. Thus the entire mesh to Si circuit appears as shown in Figure 7. Characterizing retinas for use in this program requires determining the values of the components shown in the equivalent circuit of Figure 6, and determining the range in tube bias levels over which this equivalent circuit applies. This can be done by actually measuring the target current of the tube as a function of landing voltage, silicon to mesh voltage, light level, etc.

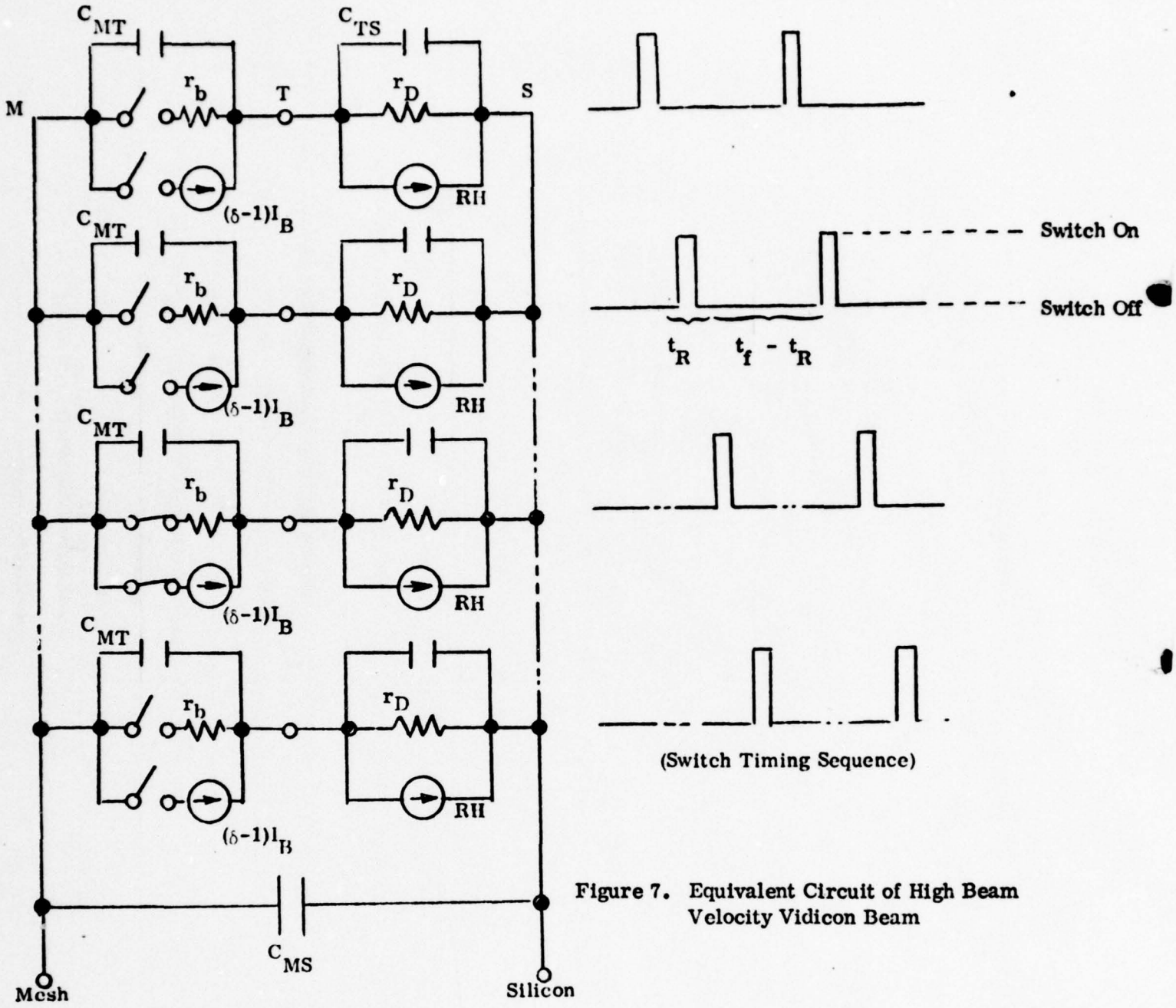

Figure 7. Equivalent Circuit of High Beam Velocity Vidicon Beam

a. D.C. Measurements

When characterizing retinas in a demountable camera tube in which the thermionic cathode is repeatedly being exposed to contamination whenever a retina is changed, it has been found that meaningful and reproducible results are best obtained when the measured target current, I_T, is normalized to the total beam current (determined by adding algebraically the total currents carried by all electrodes able to divert beam current from the retina). This obviates the need to hold cathode emission constant during a given run, or between different runs. Furthermore, the raster scan being applied should be such that the retina is underscanned, or else substantial retina edge effects result. Under these conditions, measurements of I_T vs. V_{SM} at room temperature (where r_D of Figure 6 is very low) permit the study of retina to mesh interaction under a fast beam. Figure 8 is a typical plot of such data obtained on retina 10P104. It can be seen that when the silicon (and hence at room temperature the metal islands) is positive relative to the mesh (first quadrant of Figure 8) the target current saturates at a value essentially equal to the beam current. Since the mesh transparency is only 61%, the mesh must be intercepting part of the incident beam, and emitting secondaries, some of which fall onto the retina and add to the total target current. (The presence of mesh secondaries complicates the analysis of beam-retina interaction, since they land on the target with low energy and don't generate secondaries off the retina.) Since the retina is positive relative to the mesh in this quadrant, retina secondaries cannot escape to the mesh, and the net target current consists of electron flow out the retina lead (positive current flow according to our convention).

Figure 8 also shows that when the voltage between the metal islands and the mesh is negative (third quadrant), the signal of the target current corresponds to electron flow into the tube via the retina lead. This implies that the fast beam is generating secondaries on the retina with a yield $\delta > 1$, and that these secondaries escape to the mesh when $V_{SM} \ll 0$. Useful information can be obtained about the magnitude of the secondary emission currents from an analysis of the current values at which I_T saturates for large positive and large negative values of V_{SM}.

i. Saturated Values of Target Current

Consider the structure shown in Figure 5. A fraction f_M of the incident beam

Figure 8

Normalized Target Current vs. V_{SM} ($T = 300^{o}K$, $V_{MK} = 250$ V)

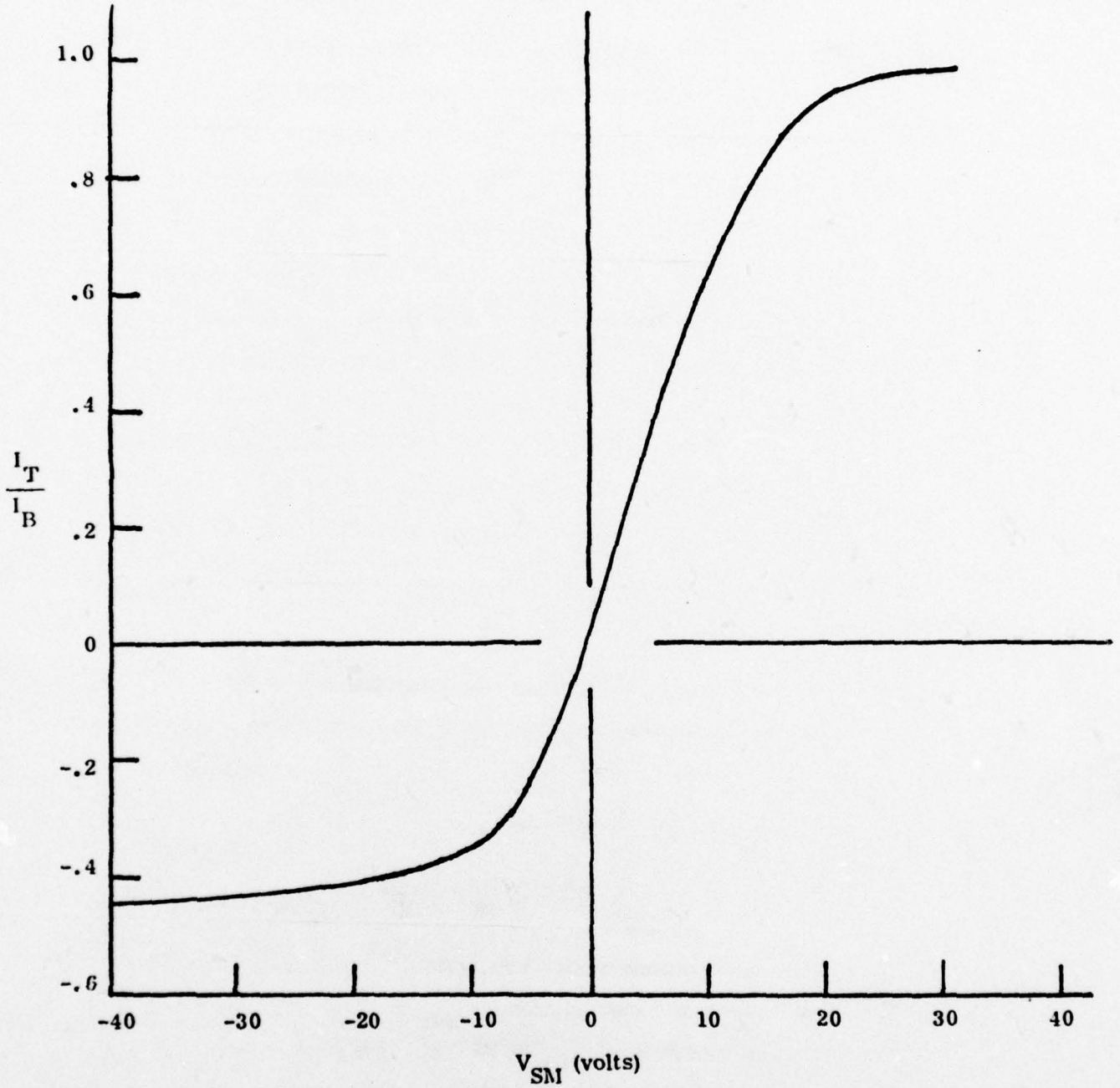

lands on the mesh and generates secondaries. For $V_{SM} \gg 0$, some of these secondaries can pass thru the mesh and land on the retina, the balance going to a remote cylindrical electrode maintained at all times at +25V relative to the mesh. If we described the yield of the mesh for secondaries going to the retina by means of the coefficient δ'_{MK}, we find that a fraction $(1 - f_M)$ of the beam current continues thru the mesh unimpeded, while the remainder is removed from the fast beam and replaced with a slow component $f_M \delta'_{MK}$. This slow component is too low in energy to create secondaries when it lands on the retina, so it tends to make the fast electrons less effective.

Of the fast electrons that pass thru the mesh, a fraction f_T land on the metal islands on the retina ($f_T = 0.64$ for diode pattern used) and generate secondaries with a yield δ_{TK}. The remainder falls on the exposed oxide. If we assume that the net current flow off the oxide surface is zero, the primaries landing there must generate an equal number of secondaries which, for $V_{SM} \ll 0$, are collected by the mesh. For $V_{SM} \gg 0$, they will be collected by the metal islands. These oxide secondaries are also unable to create secondaries, since they land on the collecting surface with low energy. Finally, the fraction of the original fast beam which can generate secondaries off the metal islands is

$$f_T (1 - f_M)$$

For $V_{SM} \gg 0$, these are unable to escape, while for $V_{SM} \ll 0$, they all escape to the mesh. By such reasoning it can be shown that the saturated values of target current should be as follows:

$$I_T/I_B = (1 - f_M) + f_M \delta'_{MK}; \quad V_{SM} \gg 0 \tag{17}$$

$$I_T/I_B = (1 - f_M) f_T (1 - \delta_{TK}); V_{SM} \ll 0 \tag{18}$$

Substituting known values for f_M and f_T into these equations, one finds from data such as that shown in Figure 8 that $\delta'_{MK} \approx 1$ (which seems reasonable in view of the inefficient collection geometry), and that δ_{TK} can be as high as 2.1 at 250 volts beam voltage. The secondary emission constants of palladium silicide are not known, but most metals show peak values of δ of the order of 1.5, and these values occur for beam voltages substantially higher than 250V. Thus, it appears that the secondary emission yield off the retinas used in this program is higher than might have been

equation (18) would predict $I_T = 0.12\ I_B$ for palladium at 250 V, while shows that $I_T = 0.45\ I_B$ was measured). We shall show later that this, with other data, forces one to the conclusion that the net current flow off the exposed oxide is not zero, but that current transport from the metal islands oxide permits the oxide to play an important role in retina-beam interaction.

The effect of retina temperature and beam landing voltage (V_{MK}) on the saturation values of target current are also of interest. Equation (17) would indicate that I_T ($V_{SM} \gg 0$) would vary with temperature and voltage as the secondary emission yield of the copper mesh does, i.e., I_T ($V_{SM} \gg 0$) would be expected to show no strong dependence on either variable. This in fact is what is observed (Cf. Figure 9A). I_T ($V_{SM} \ll 0$) should depend on T and V_{MK} as δ_{TK}, the secondary emission yield of the target. Figure 9B shows a comparatively strong dependence on both T and V_{MK}. Once again there is indication that the secondary emission characteristics of the retina surface are more like those of an insulator than a metal.

ii. Evidence for Beam Induced Conductivity in Exposed SiO_2 on Retina Surface

At low values of beam landing voltage ($V_{MK} < 100$ volts) hysteresis effects were observed in the measurement of I_T. This data is best presented by plotting I_T (normalized as before to I_B, the total beam current) vs. the total target to cathode voltage (V_{TK}). Figure 10 shows such a plot for retina 10P113. The data was taken with the retina at room temperature, and with the electron beam unscanned (beam focused on the same spot on the retina throughout the measurement), although similar data has been obtained with the retina cold, and with the beam being scanned in the normal raster fashion.

Several points of interest can be noted from Figure 10. First, the average retina (δ_{TK}) of secondary electrons is greater than one for both branches of the curve $\gtrsim 75$ volts. (This follows from the fact that the signal of the target current is) Second, $\delta_{TK} > 1$ for $V_{TK} \gtrsim 30$ volts for the lower branch. Both of these are surprising in view of the fact that the landing voltage at which $\delta \to 1$ is, for usually in the neighborhood of 100-300 volts. On the other hand, silicon has a value of 30 volts for the first crossover voltage (V_C), and δ reaches a of 2.1 to 2.9 for a voltage of 400-440 volts.[13] Both the data of Figure 10

Figure 9

Saturated Target Current vs. V_{MK}

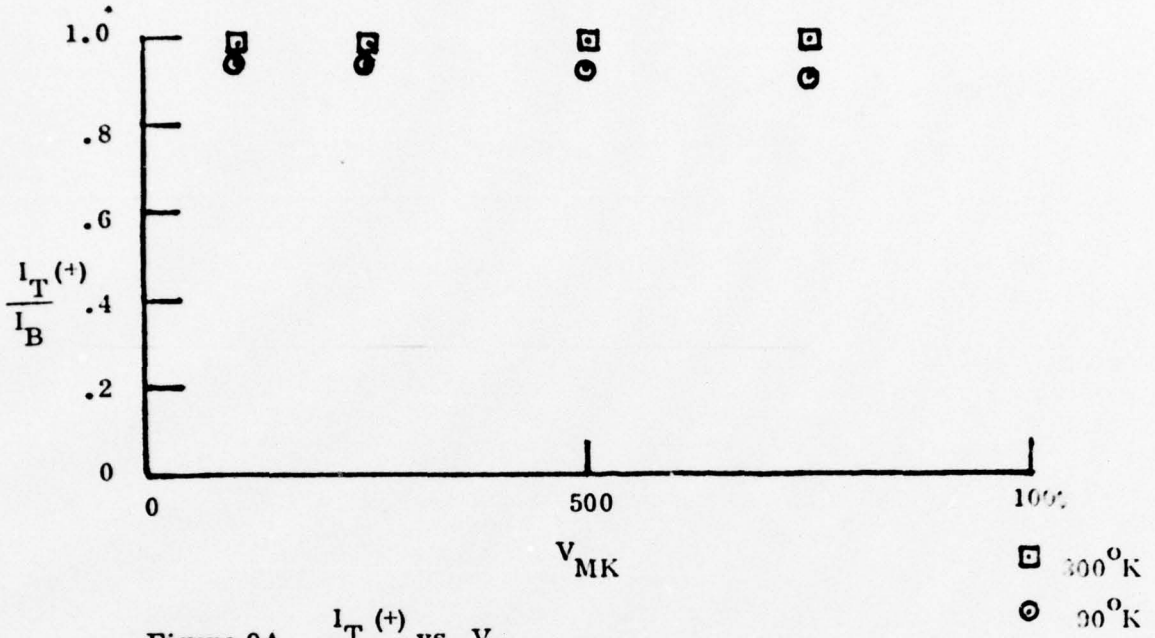

Figure 9A. $\frac{I_T(+)}{I_B}$ vs. V_{MK}

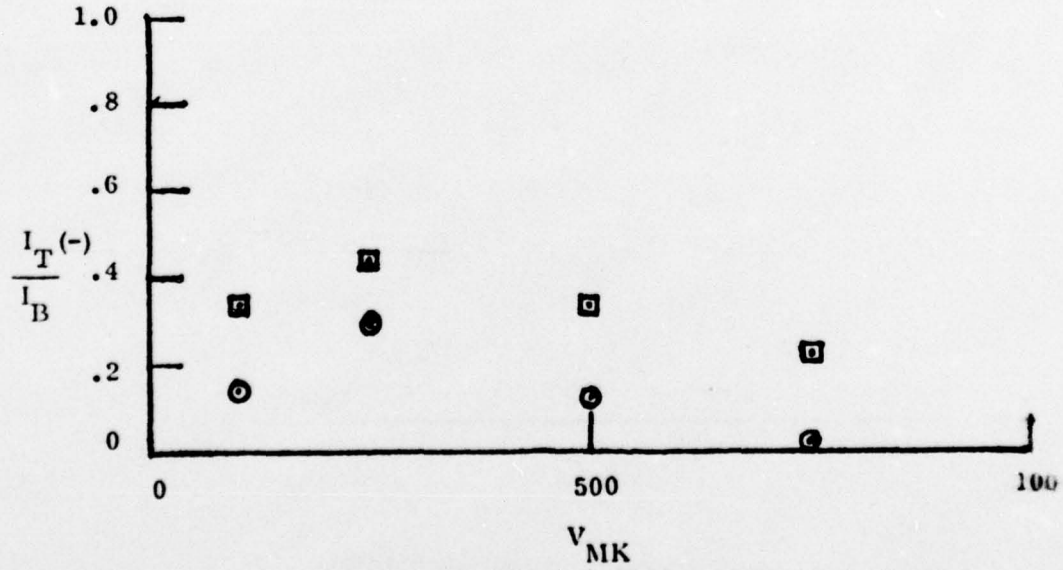

Figure 9B. $\frac{I_T(-)}{I_B}$ vs. V_{MK}

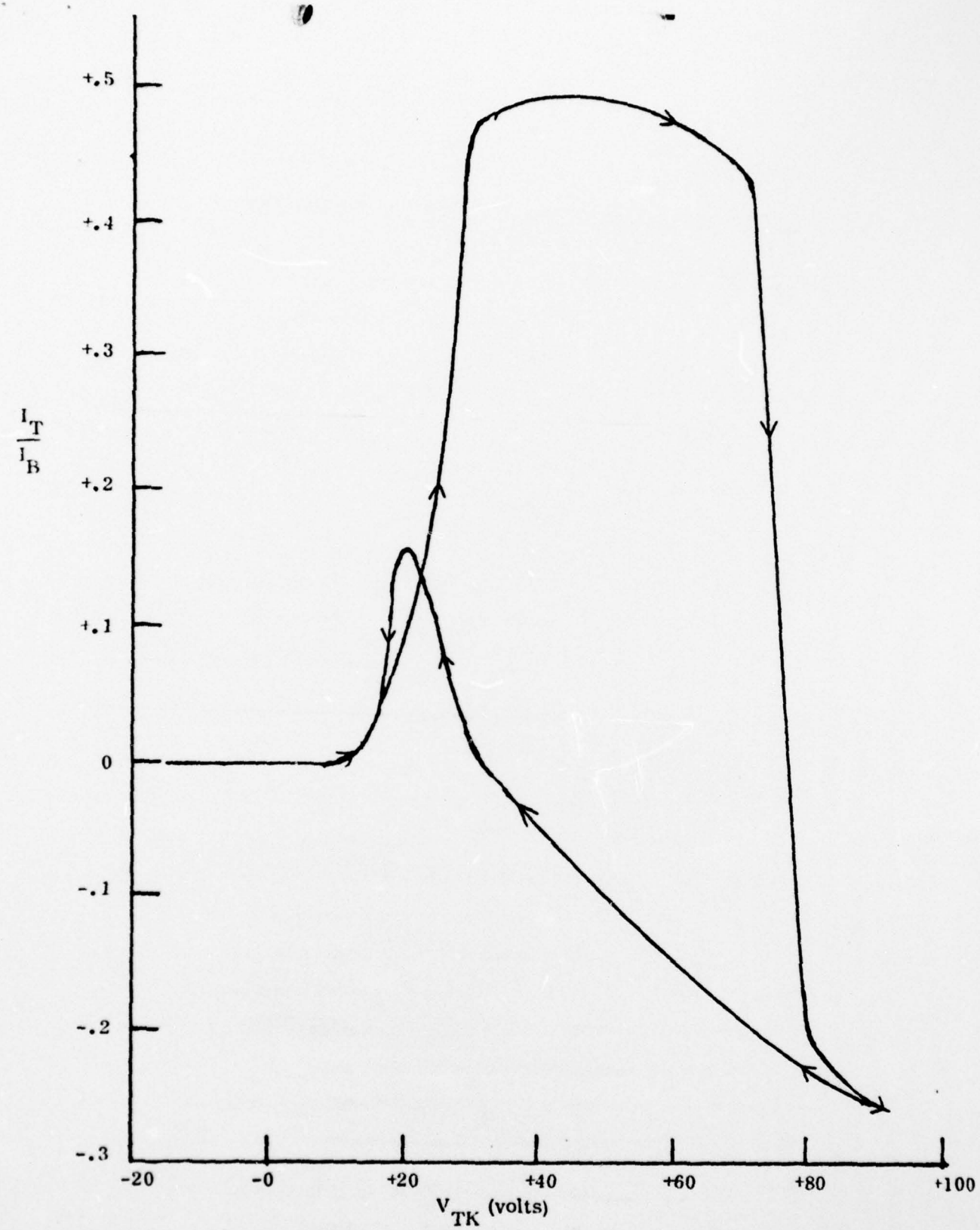

Figure 10. Normalized Target Current vs. V_{TK}
(Unscanned, T = 300°K)

and that of 9B are in closer agreement with the properties of SiO_2 than with those of any known metal (including palladium and silicon).

The third point of interest in the data of Figure 10 lies in the fact that the data was obtained on a D.C. basis. The conventional methods used to determine the secondary emission properties of insulators involve A.C. techniques, since the secondary electrons cannot be replaced by normal conduction processes, so that the targets charge to whatever potential will permit them to have no net current. (Insulators charge to cathode potential if $V_{TK} < V_C$, and to a voltage $\overline{V}$ $\ell n\ \delta$ above mesh potential if $V_{TK} > V_C$). It is obvious that for the SiO_2 to be playing the role in secondary emission from the retina which the data of Figures 9B and 10 would indicate, it must be conducting (at least in the presence of the beam), and there must be a contact to it capable of supplying electrons to the conduction band of the oxide to replace those lost by secondary emission. If we assumes that the beam does induce conductivity in the oxide, and that the metal-oxide interface, while under the beam, is capable of supplying electrons to the conduction band of the oxide, it becomes relatively straightforward to explain the hysteresis shown in Figure 10.

3. Retina Photoresponse Measurements Using Electron Beam Contact

The previous section dealt with the secondary emission properties of Schottky barrier retinas deduced from measurements of D.C. target current, performed (usually) at room temperature. Under these conditions the impedance of the Schottky diode can be assumed to be negligible, so that the entire values of V_{SM} falls across the vacuum gap between metal and mesh (or across the parallel path between silicon and mesh, through the silicon dioxide layer). As the retina temperature is reduced, however, the impedance of the Schottky diode rises, and a portion of V_{SM} can drop across the diode. It should then be possible to determine the dark current of the retina by measuring D.C. target current, I_T, vs. V_{SM} at low temperatures. Furthermore, measurements of I_T vs. V_{SM} at various light levels up to that value required to saturate the tube will provide information on tube dynamic range, linearity, and absolute responsivity.

Figure 11 is a plot of I_T vs. V_{SM} for retina 10P115, obtained with the retina at operating temperature ($T < 100^{\circ}K$). Curve 1 was obtained under "dark" conditions, i.e., no radiation was intentionally introduced. (Thermal radiation from tube surfaces

Figure 11

$\frac{I_T}{I_B}$ vs. V_{SM} for Retina 10P115

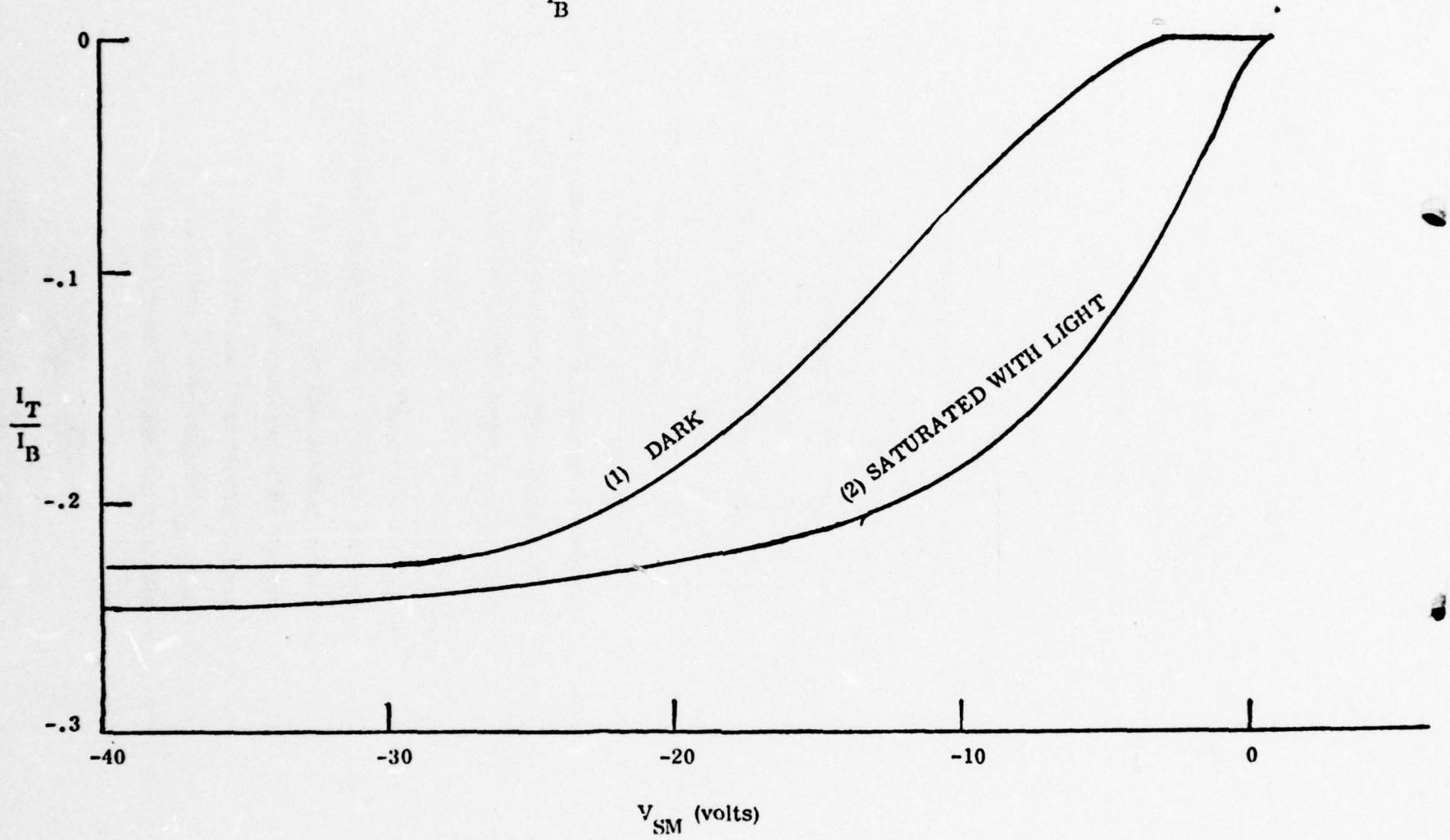

at room temperature, such as the quartz window, cannot presently be excluded). Curve 2 was taken under saturated light conditions, i.e., at light levels sufficiently high that no further increases in I_T occurred. Neglecting the slight separation between the curves for large negative values of V_{SM} (not yet explained), the shape of the curves is as expected. I_T on curve 1 is limited by diode impedance for low negative values of V_{SM}. As $|V_{SM}|$ increases, however, diode impedance begins to decrease until, for $|V_{SM}| > 25$ volts, it has decreased to the point where beam impedance again limits I_T. Thus, measurements of I_T vs. V_{SM} at operating temperatures provide information on diode dark current under actual operating conditions. Figure 12 shows such curves for retina 10P104 for several different values of beam landing voltage. This data shows that the value of V_{TM} at which I_T changes sign is dependent upon V_{MK}. This is not surprising, since the crossover point depends in a complicated way on δ'_{MK} and δ_{TK}, the secondary emission yields of the mesh and the retina surface. It is clear, however, that the diode voltage drop is zero at the crossover point V_O, and the diode becomes reverse biased as V_{SM} is decreased below V_O. Figure 12 shows that substantial evidence of high diode impedance is seen out to $V_{SM} = -10$ volts for $V_{MK} = +250$ volts, but at higher values of V_{MK}, the diode impedance decreases, and has essentially vanished at 750 volts V_{MK}. This would be expected if the metal islands (or the SiO_2) were sufficiently thin that at high voltages, a fraction of the beam could penetrate thru this layer and enter the silicon, there discharging the diode by the creation of hole-electron pairs. Care must be exercised, therefore, in estimating retina leakage current from target current measurements, since V_{MK} plays an important role.

Considering the 250 volt curve in Figure 12, it can be seen that the diode leakage at $V_{SM} = -10$ volts must be 12 na or less. This is quite low, considering that the scanned area was 5.8 cm^2, and shows that Schottky retina leakage can be reduced to a sufficiently low level, under actual conditions of retina temperature and high velocity scanning, to permit vidicon operation. Future retina designs will concentrate on maintaining this low leakage over a wide range of V_{SM} (higher breakdown diodes) and a wider range of V_{MK} (thicker metal islands, thicker oxides, closer control over surface scratches).

Figure 12

Target Current, I_T vs. V_{SM} for Various V_{MK}

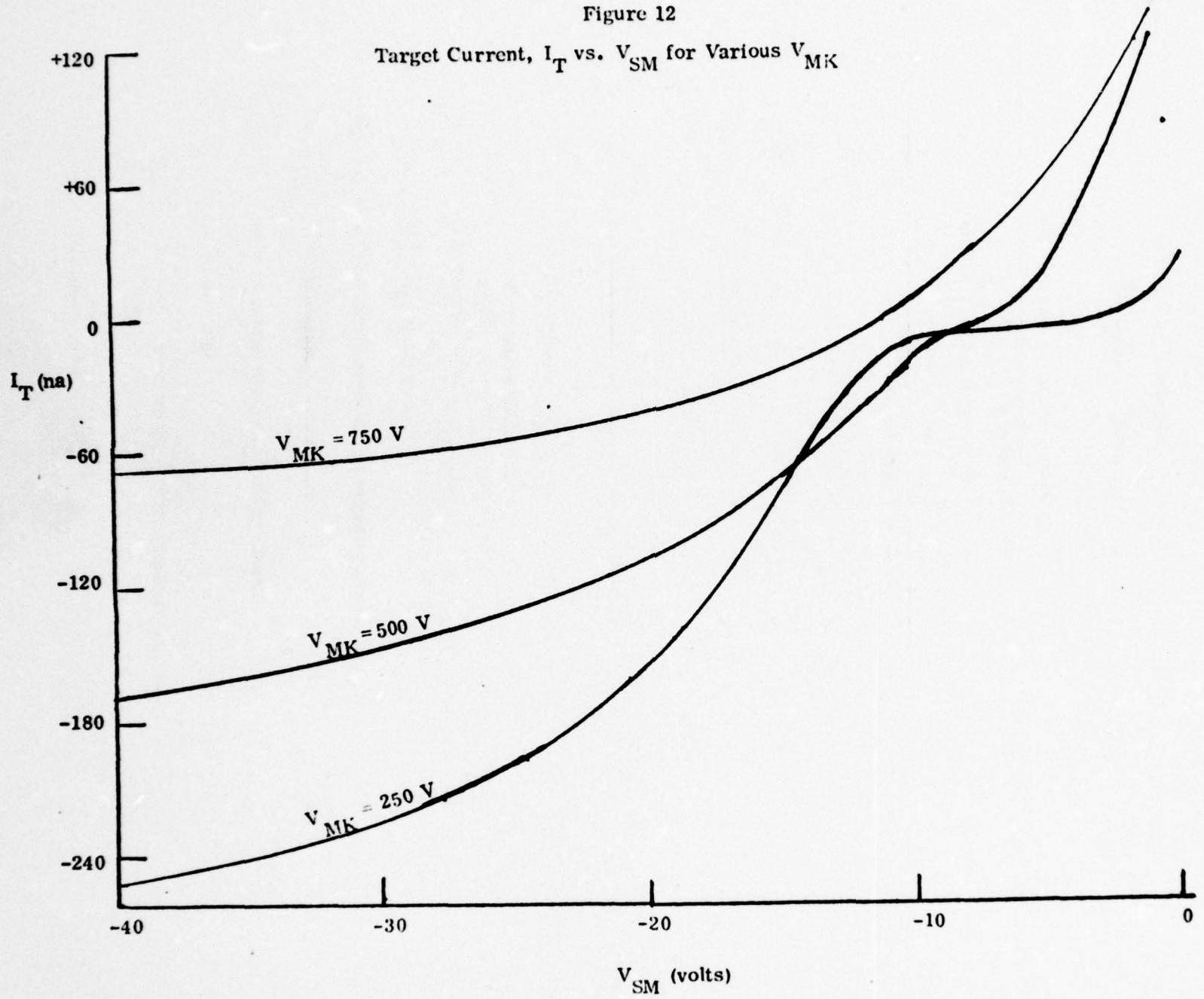

Measurements of I_T vs. V_{SM} at various levels of uniform retina illumination permit the determination of tube responsivity, linearity, and dynamic range. Figure 13 is a plot of such data obtained on retina 10P115. Curve 0 is the dark curve, curves 1 thru 3 show I_T under illumination from an 800^{o}K black body (irradiances were .1 P_o, .5 P_o, and P_o, where $P_o = 8.9 \times 10^{-5}$ watts). Curve 4 is a saturated curve obtained using a microscope lamp operated sufficiently hot to saturate the retina. This data shows that the dynamic range of the retina is limited at the low end by retina dark current, I_D, and at the high end by the maximum target current that the beam can supply. The latter quantity doesn't saturate with voltage until $|V_{SM}| > 20$ volts. Thus, it would be desirable if the retina dark current could be maintained at a low value until beam saturation occurs, since this would assure maximum dynamic range. This is equivalent to requiring that retina diode breakdown be ≥ 20 volts.

Retina responsivity and linearity can be obtained from the data of Figure 13. Figure 14 is a plot of the photocurrent I_S at $V_{SM} = -10$ volts (target current minus dark current) normalized to the maximum photocurrent that can flow (saturated target current minus dark current). This data shows that the target photocurrent varies linearly with signal irradiance, i.e., $\gamma = 1$ in the equation

$$I_T - I_D = R\,(f_T H_S A_{raster})^{\gamma} \tag{19}$$

where I_T = target current under illumination

I_D = target current in dark

R = proportionality constant

H_S = signal irradiance incident on Schottky diodes in watts/cm^2

A_{raster} = scanned area of retina

f_T = fraction of retina area occupied by diodes

γ = linearity constant

Since $\gamma = 1$, R can be interpreted as the retina responsivity. The value of R calculated for retina 10P115 from the data of Figure 13 is

$R = 0.8$ ma/watt

Figure 13

Normalized I_T vs. V_{SM} at Various Light Levels

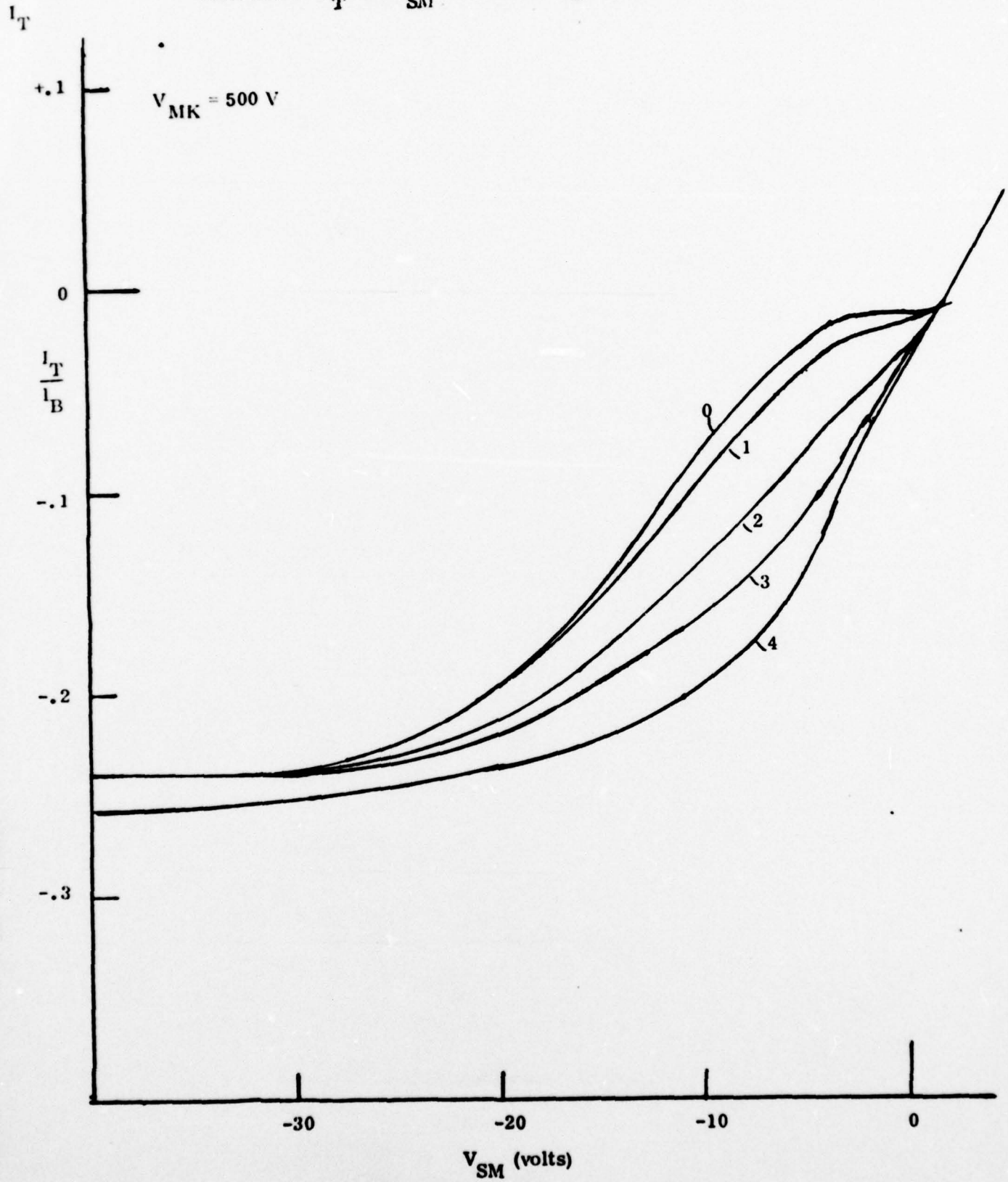

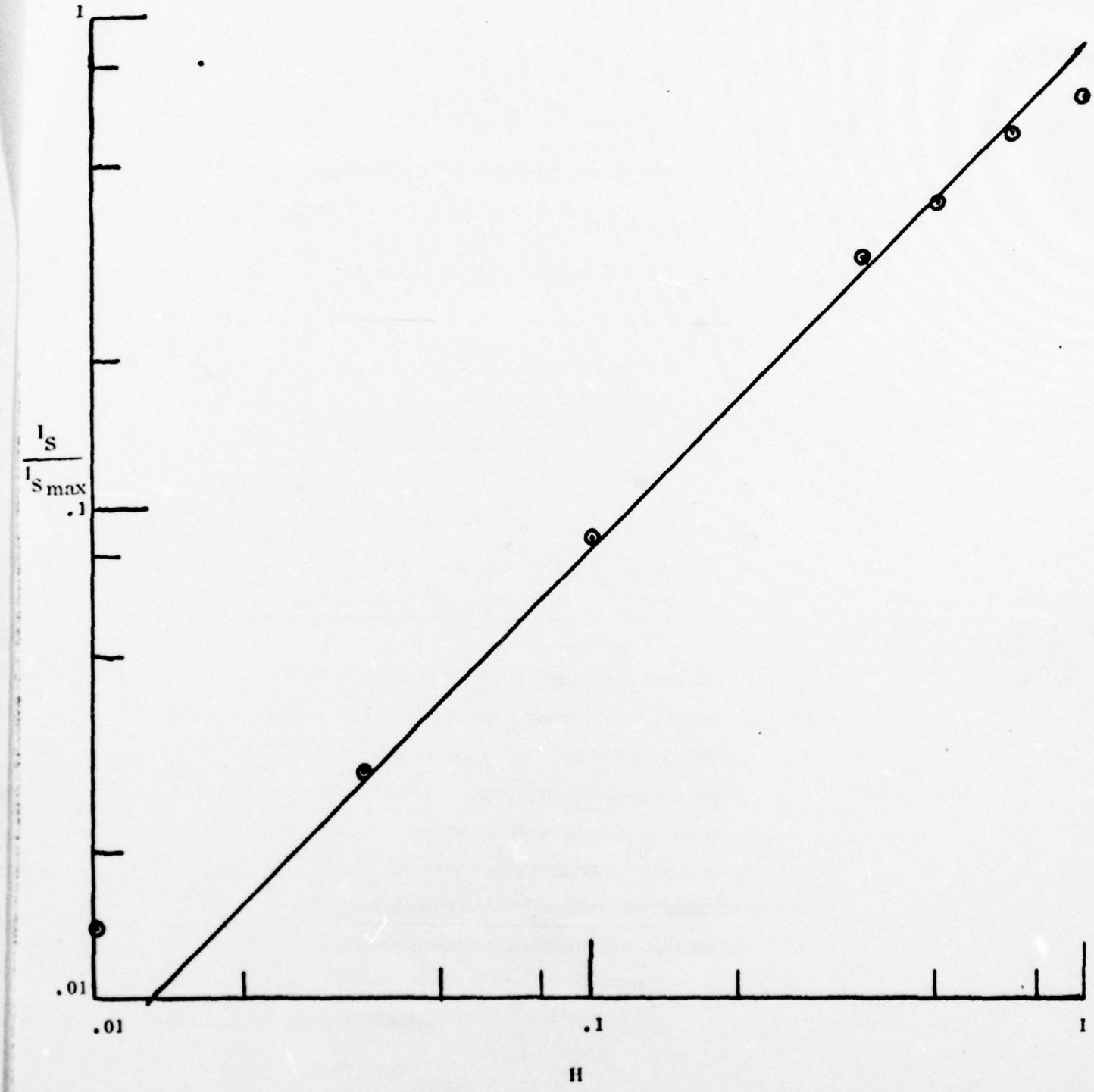

Figure 14. Retina Photocurrent vs. Radiance.

The theoretical value for responsivity of a Schottky barrier internal photoemissive detector for a black body of temperature T is[14]

$$R(T) = \frac{30 C_1}{\pi^4} \left(\frac{q\phi_o}{kT} + 3 \right) \exp\left(- \frac{q\phi_o}{kT} \right) \qquad (20)$$

where C_1 = quantum efficiency coefficient found for these retinas to be $\sim$ 0.04 amperes/watt

ϕ_o = Schottky barrier height

For T = 800°K, R(T) calculated from equation (20) is, for ϕ_o = 0.35 eV,

R(T) = 0.62 ma/watt

The agreement is seen to be quite good.

III. IMAGING WITH INFRARED VIDICON CAMERAS

A. Theory

The infrared vidicon is, under usual operating conditions, an irradiance sensor rather than a power sensor. To explain this statement, consider a typical line of video information displayed on an 'A' scope (Cf. Figure 15). This line might be one obtained from the video processor while an image of a vertical bar is being displayed. The "front porch," "back porch," and sync tip portions of this waveform perform the same function in an infrared vidicon camera system that they do in standard television systems. The portion of this line of information which contains information about the scene is that between t_3 and t_6. For most of this time the signal level is at the dark level. Between t_4 and t_5, the signal level is at a value determined by the signal irradiance at the retina, the responsivity of the retina, etc. If the width of the vertical bar being imaged is increased without changing its radiant emittance, the height of the signal seen on the A scope would not increase, but the width, $t_5 - t_4$, would. This is described by the following equation for I_T, the target current flowing thru the input resistor of the pre-amplifier.

$$I_T = I_D + \frac{R f_T H_S A_{raster}}{\left(1 + A_e/A_i\right)} \qquad (21)$$

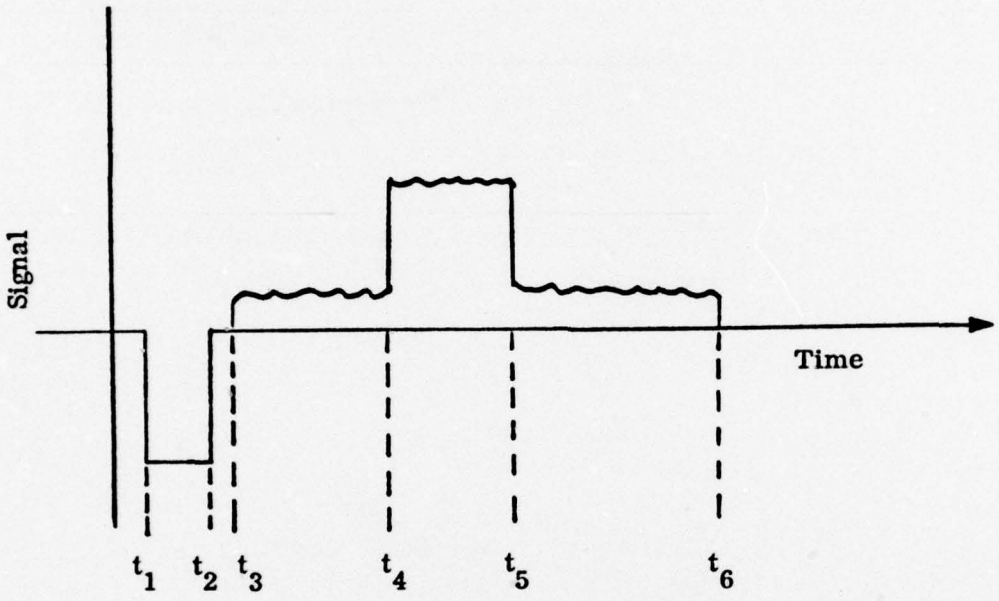

Figure 15. Line of Video (as shown on A scope thru center of image of vertical bar)

where I_D = dark current

R = responsivity of Pd_2Si/p-silicon Schottky diode

f_T = fraction of retina surface covered by diodes (f = .64 here)

H_S = signal irradiance at sensing layer

A_{raster} = area of raster scan

A_e = resolution element size

A_i = image area

[The term $(1 + A_e/A_i)$ takes into account the fact that in the limit of very small area images, full storage mode gain cannot be achieved.] To obviate the need to monitor system gain continually, signal-to-noise ratio is usually measured rather than signal current. Thus

$$\frac{S}{N} = \frac{I_T - I_D}{i_N} = \frac{R f_T H_S A_{raster}}{\left(1 + \frac{A_e}{A_i}\right) i_N} \tag{22}$$

where i_N = equivalent input noise current

1. Signal Levels

a. Optics

The signal irradiance H_S incident on a retina as a result of exposure to a black body of temperature T is[15]

$$H_S = \frac{W_{BB} T_A T_O}{4F^2 (M + 1)^2} \tag{23}$$

where W_{BB} = radiant emittance of black body in watts/cm^2

T_A = transmission of atmosphere

T_O = transmission of optics

F = F# of optical system

M = magnification of optics

For the experiments described herein the F# of the optics could be varied by means of an iris from a maximum of 26.7 to a minimum of 3.5, to permit continuous variation of H_S over 1-1/2 decades. The magnification used was measured directly, and was in the range from 0.38 to 1. T_A was assumed to be one, while T_O was calculated from the known absorptances and reflectances of all the elements in the optical path. Figure 16 shows T_O vs. λ for the optics used in the feasibility experiments.

b. Retina Responsivity

Retina responsivity can be determined either of two ways, viz. the responsivity to a black body of temperature T (Cf. equation 20), or spectral responsivity $R(\lambda)$.

$$R(\lambda) = C_1 \left(1 - \frac{\phi_o}{h\nu}\right)^2 = C_1 \left(1 - \frac{\phi_o \lambda}{1.24}\right)^2 \; ; \; \lambda \leq \frac{1.24}{\phi_o \text{ (eV)}}$$

$$R(\lambda) = 0 \; ; \; \lambda > \frac{1.24}{\phi_o \text{ (eV)}} \qquad (24)$$

where C_1 = quantum efficiency coefficient, found to be 0.04 amps/watt in this program

ϕ_o = Schottky barrier height (eV)

Figures 17 and 18 show R(T) vs. T and $R(\lambda)$ vs. λ for the Pd_2Si/p-type silicon retinas used in this program, and the PtSi/p-type silicon retinas to be used to extend this concept to the 5 micron region.

c. Raster area

It is clear from equation (22) that the size of the raster should be as large as possible to take maximum advantage of storage mode gain. The largest value of A_{raster} that can be utilized effectively is that which can be scanned in a frame time by an electron beam of size A_e (assumed to be adjusted to equal overall system resolution element size).

$$A_{raster|MAX} = \frac{t_F}{t_R} A_e \qquad (25)$$

where $A_{raster|MAX}$ = maximum usable scanned area

Figure 16. System Transmittance vs. Wavelength

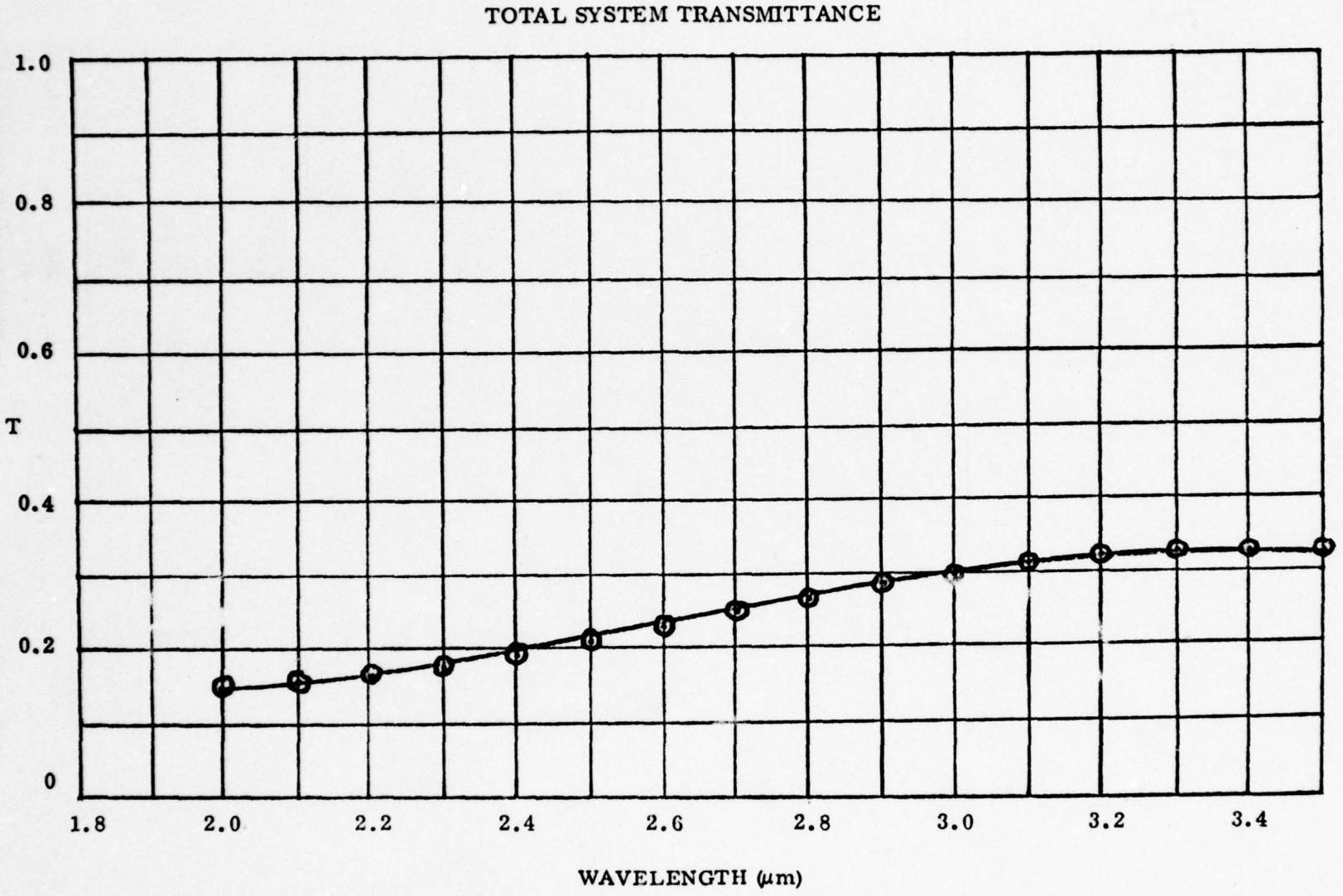

Responsivity vs. Black Body Target Temperature
for Schottky Barrier Retina

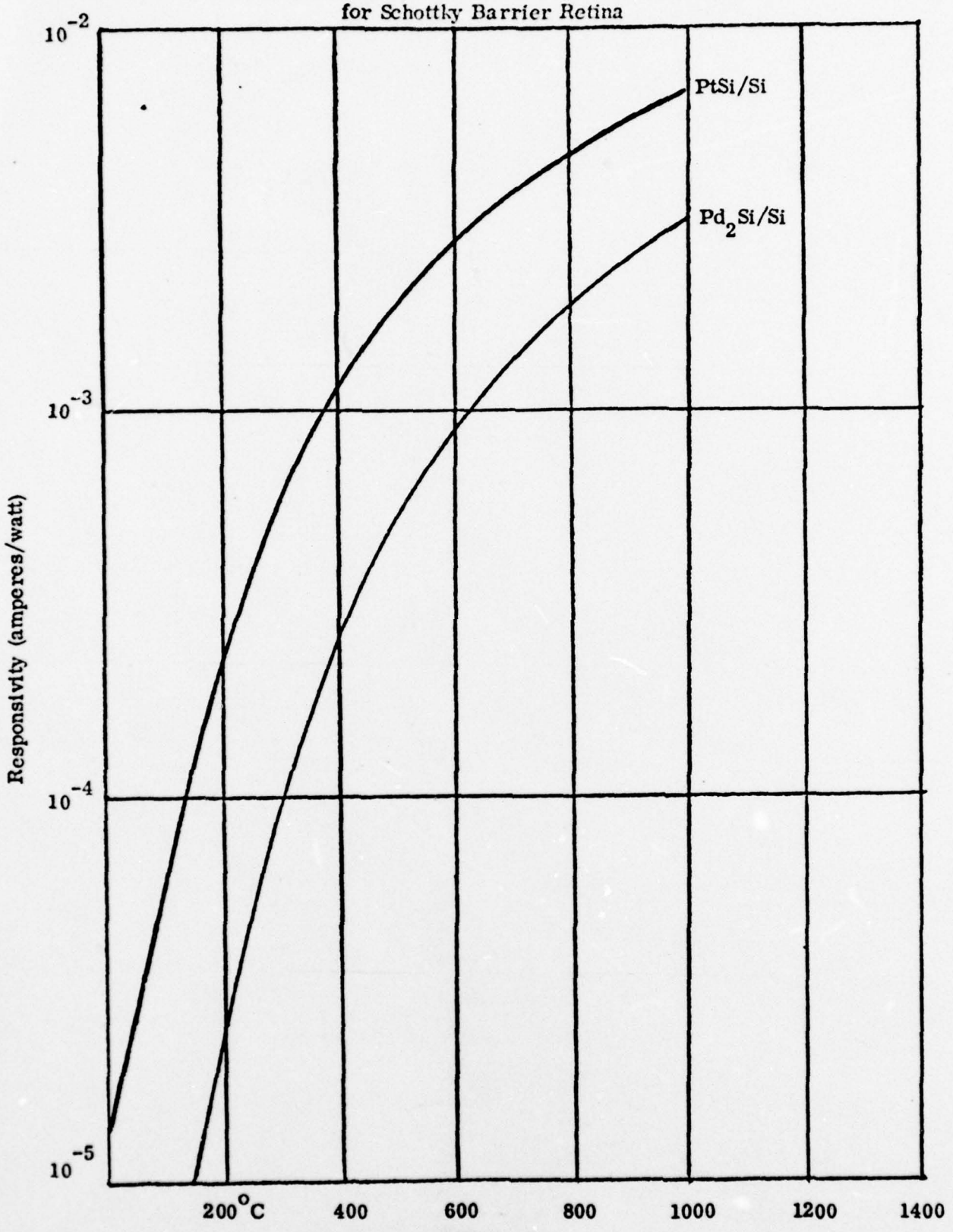

Spectral Responsivity of Schottky Diodes

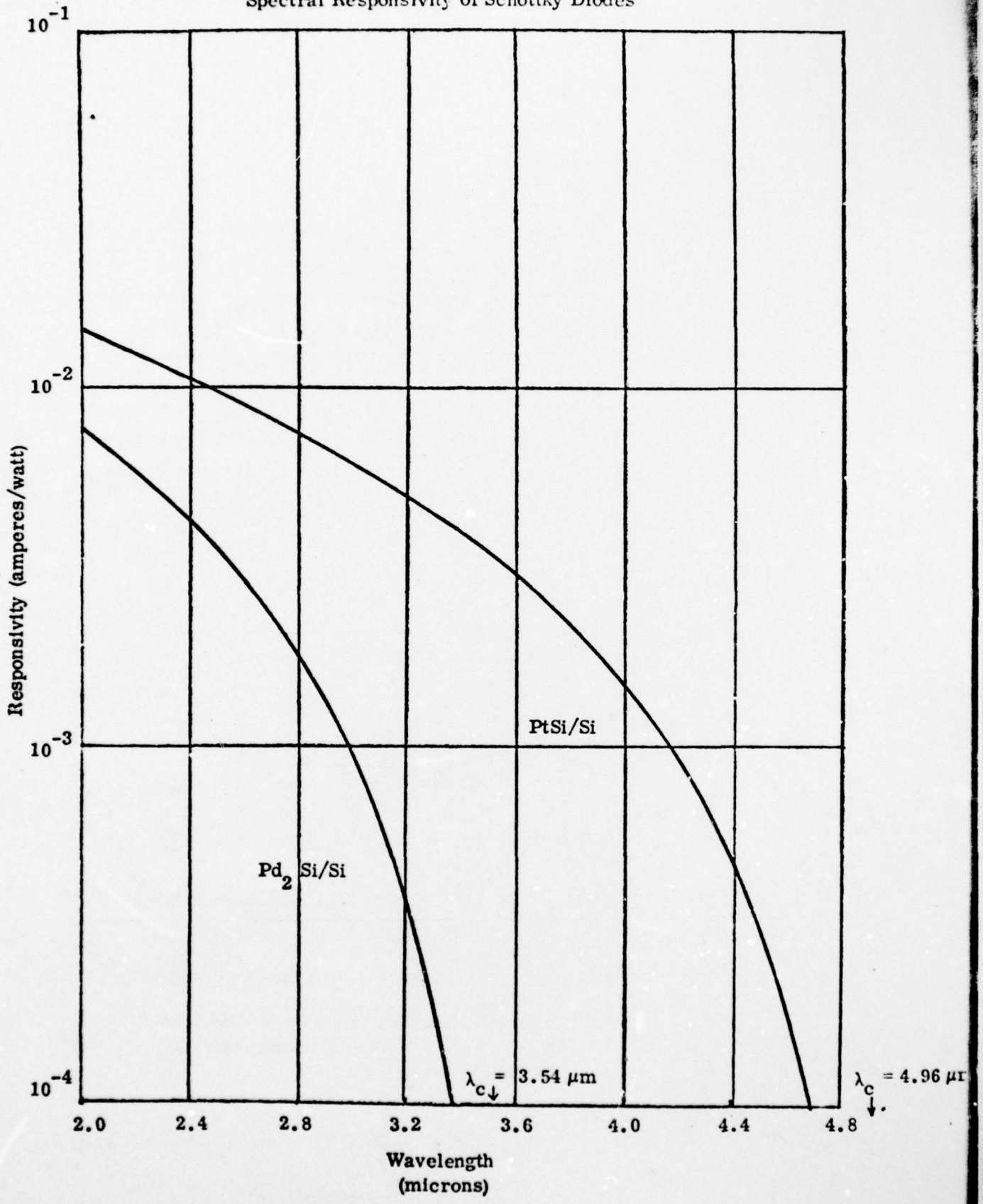

A_e = resolution element size

t_f = frame time (maintained at 1/30 sec in this study)

t_R = read time = $1/(2\ \Delta f)$

Δf = system bandwidth (usually kept at 4.5×10^6 Hz)

Since $A_{raster|MAX}$ is determined by retina technology, A_e by beam-retina interactions, and t_f by the standard frame rate, noise bandwidth is thus determined by equation (25). This equation also determines system resolution, since the number of TV lines which can be resolved in a square format picture is given by

$$N = \left(\frac{A_{raster}}{A_e}\right)^{1/2} \tag{26}$$

2. Noise

Noise in the trace shown in Figure 15 can arise from several sources, viz. pre-amplifier noise, shot noise in the beam, fixed pattern noise due to point-to-point variations in retina properties, etc. To determine the magnitude of each of these noise sources, it is helpful to consider the equivalent circuit representing what the pre-amplifier sees looking back into the tube (Cf. Figure 19). The elements in this equivalent circuit are defined as follows.

Element ij is the picture element under the scanning beam at time t.

A_e is the area of picture element ij.

C_{MT} is the collector mesh to target surface capacitance of element ij.

$$C_{MT} = \frac{\epsilon_o A \epsilon f_M}{d_{MT}} \tag{27}$$

d = mesh to target surface spacing

f_M = fraction of the mesh which is able to contribute to mesh capacitance (f_M is the opacity of mesh)

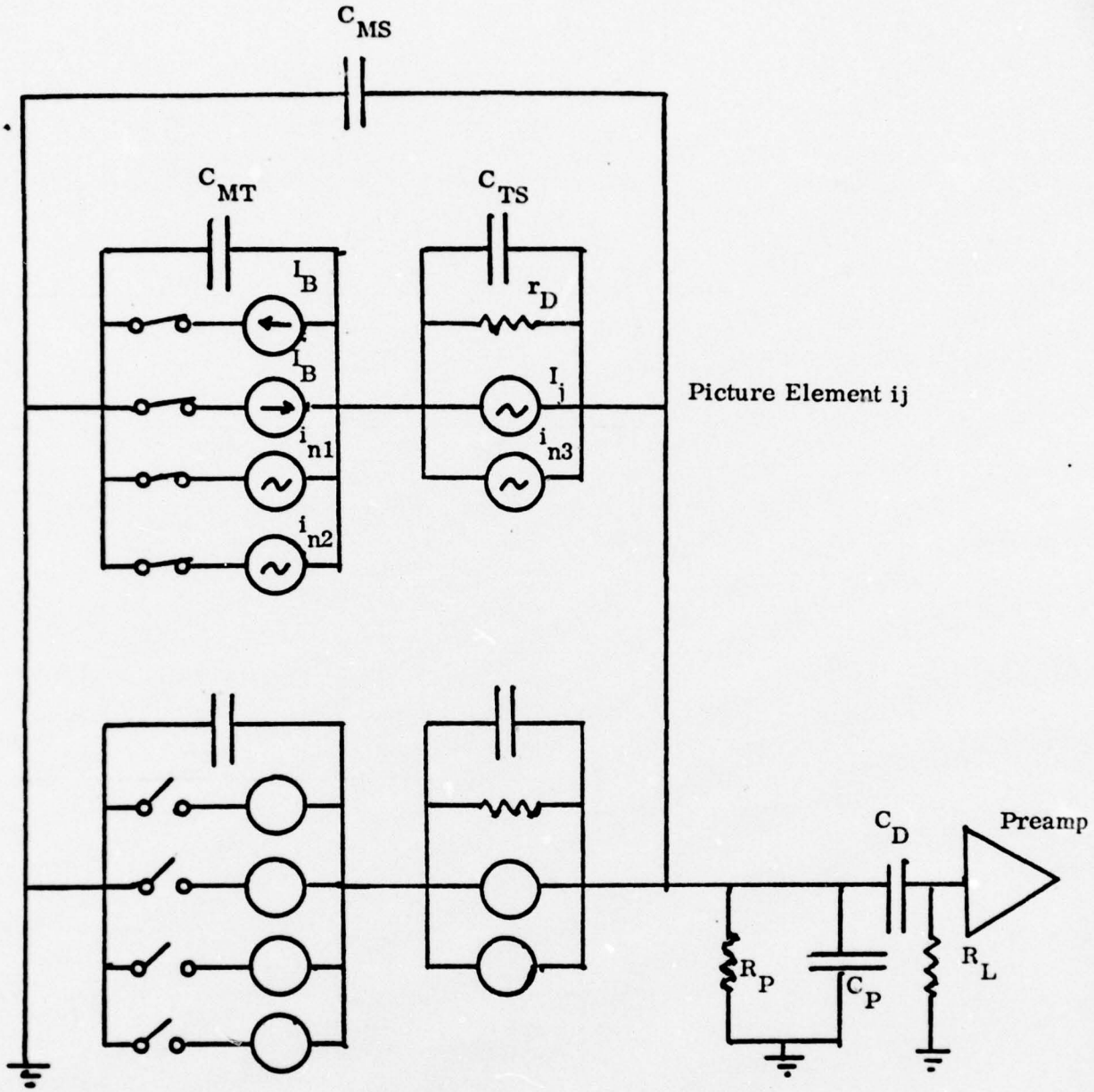

Figure 19. Equivalent Circuit of Retina and Tube as Seen from Preamp

I_B = beam current incident on retina surface

I'_B = secondary emission current from retina to mesh

$$I'_B = \delta I_B \exp(-V_{FT}/\overline{V}) \tag{28}$$

i_{n1} = noise associated with I_B

$$i_{n1} = [2q I_B \Delta f] \tag{29}$$

$$\Delta f = 1/2\, t_R \tag{30}$$

t_R = time beam dwells on element ij.

i_{n2} = noise associated with secondary emission from retina to mesh. Since I'_B can vary from I_B to δI_B as the light level incident on the retina varies from zero to saturation, i_{n2} will vary. For a worst case evaluation we shall assume that $I'_B = \delta I_B$. Then

$$i_{n2} = [2q\delta^2 I_B \Delta f]^{1/2} \tag{31}$$

C_{TS} is the silicon to target surface capacitance of element ij.

$$C_{TS} = \frac{K_{Si}\, \epsilon_o\, A_e\, f_T}{d_{TS}} \tag{32}$$

K_{Si} = dielectric constant of silicon

f_T = fraction of retina surface occupied by Schottky diodes

d_{TS} = width of depletion layer of Schottky diode

r_D is the reverse resistance of the Schottky diodes in element ij.

I_j is the total current carried by the Schottky diodes in element ij.

$$I_j = I_L + RH_S A_e f_T \tag{33}$$

I_L = reverse leakage current of Schottky diodes in element ij

R = responsivity of diodes in ij

H_S = irradiance incident on retina

i_{n3} = noise associated with diode photocurrent

$$i_{n3} = \left[\frac{q\, I_j}{t_F}\right]^{1/2} \tag{34}$$

For worst case considerations, we shall assumed that $I_j = I_B$

t_f = frame time of camera tube

R_P = internal leakage resistance of tube

C_P = internal parasitic capacitance of tube

C_B = blocking capacitance

R_L = load resistance of retina

C_{MS} is the collector mesh to silicon capacitance.

If we assume that the retina is in the cyclic state, i.e., the beam returns the retina to the same state of charge on each frame, this can be simplified to the equivalent circuit shown in Figure 20, where

i_{n1} = effective noise current of secondary emission process

$$= [2q\, I_B (1 + \delta^2)\, \Delta f]^{1/2} \tag{35}$$

i_{n2} = background noise

$$= \left[\frac{q\, I_B}{t_F}\right]^{1/2} \tag{36}$$

i_{n3} = "spatial noise" of retina, i.e., point-to-point variations in target current under uniform illumination

$$= g I_B \tag{37}$$

where g is the r.m.s. spatial variation in target current.

i_{n4} = Johnson noise in retina load resistor R_L at temperature T_L

$$= [4kT_L\, \Delta f / R_L]^{1/2} \tag{38}$$

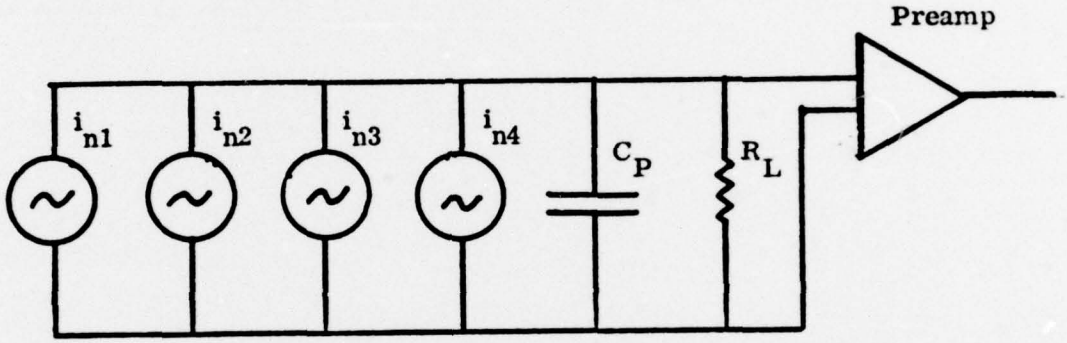

Figure 20. Noise Equivalent Circuit of High Beam Velocity Vidicon

It can be seen that $i_{n2} \ll i_{n1}$. Thus we can neglect background noise.

a. . Beam Noise

As stated in equation (35),

$$i_{n1} = [2q I_B (1 + \delta^2) \Delta f]^{1/2} \tag{39}$$

In order to avoid detector saturation when operating against a background temperature of T_b, the camera tube must be capable of replacing retina charge leaked off by background radiation. Thus, combining equations (20), (23), and (26), we can determine I_B for various values of retina parameters.

$$I_b = \frac{W_{bb}(T_b)\, T_A T_O}{4F^2 (M+1)^2}\, R(T_b) f_T N^2 A_e \tag{40}$$

Experimental data obtained on Schottky barrier retinas shows that $\delta \approx 2$ (Cf. Figure 8). Further, the noise bandwidth is related to system resolution, N, by the equation

$$\Delta f = \frac{N^2}{2t_F} \tag{41}$$

Thus,

$$i_{n1} = \left[\frac{2q(1+\delta^2) W_{bb}(T_b)\, T_A T_O}{4F^2 (M+1)^2}\, \frac{R(T_b) f_T A_e N^4}{2t_F} \right]^{1/2} \tag{42}$$

b. Spatial Noise

In going from Figure 19 to Figure 20, the collection of picture elements (all having slightly different values of R, δ, etc.) was replaced by a single picture element having a spatial noise current generator associated with it of magnitude.

$$i_{n3} = g I_B \tag{43}$$

where I_B is given by equation (40).

c. Johnson Noise in Load Resistor

As stated in equation (38),

$$i_{n4} = \left[\frac{4kT_L \Delta f}{R_L} \right]^{1/2} \tag{44}$$

The upper limit on R_L is that set by the time constant of the pre-amp input. Thus (neglecting the use of high frequency peaking circuits),

$$\Delta f = \frac{1}{2\pi R_L C_P} \tag{45}$$

In a well designed infrared vidicon tube, C_P can be made as low as 10 pf.[16] Thus,

$$i_{n4} = [8\pi k T_L C_P]^{1/2} \Delta f$$

$$= [8\pi k T_L C_P]^{1/2} \frac{N^2}{2t_F} \tag{46}$$

d. Total Noise

The total noise in the system is given by

$$i_n = [i_{n1}^2 + i_{n3}^2 + i_{n4}^2]^{1/2} \tag{47}$$

Figure 21 shows beam current, I_B, and total noise current, i_n, vs. N, system resolution in TV lines per raster height (assuming square format) for a Schottky barrier infrared vidicon of cutoff wavelength 3.5 μm (Pd_2Si/p-type silicon retina). In this spectral range, i_n is determined by pre-amplifier noise, so that the retina uniformity factor, g, has little effect on system noise. Figure 22 shows similar data for a 5 μm cutoff tube (PtSi/p-type silicon retina). Here, spatial noise limits tube performance for values of $g \gtrsim .001$.

3. Signal-to-Noise Ratio

Returning to equation (22), we see that evaluation of infrared vidicon retinas consists of determining the factors affecting the equation.

$$\frac{S}{N} = \frac{R f_T H_S A_{raster}}{i_n \left(1 + \frac{A_e}{A_i}\right)} \tag{48}$$

Figure 21. Beam Current and Noise Current vs. Resolution (Raster Size) for SBIRV (λ_C = 3.5 μm)

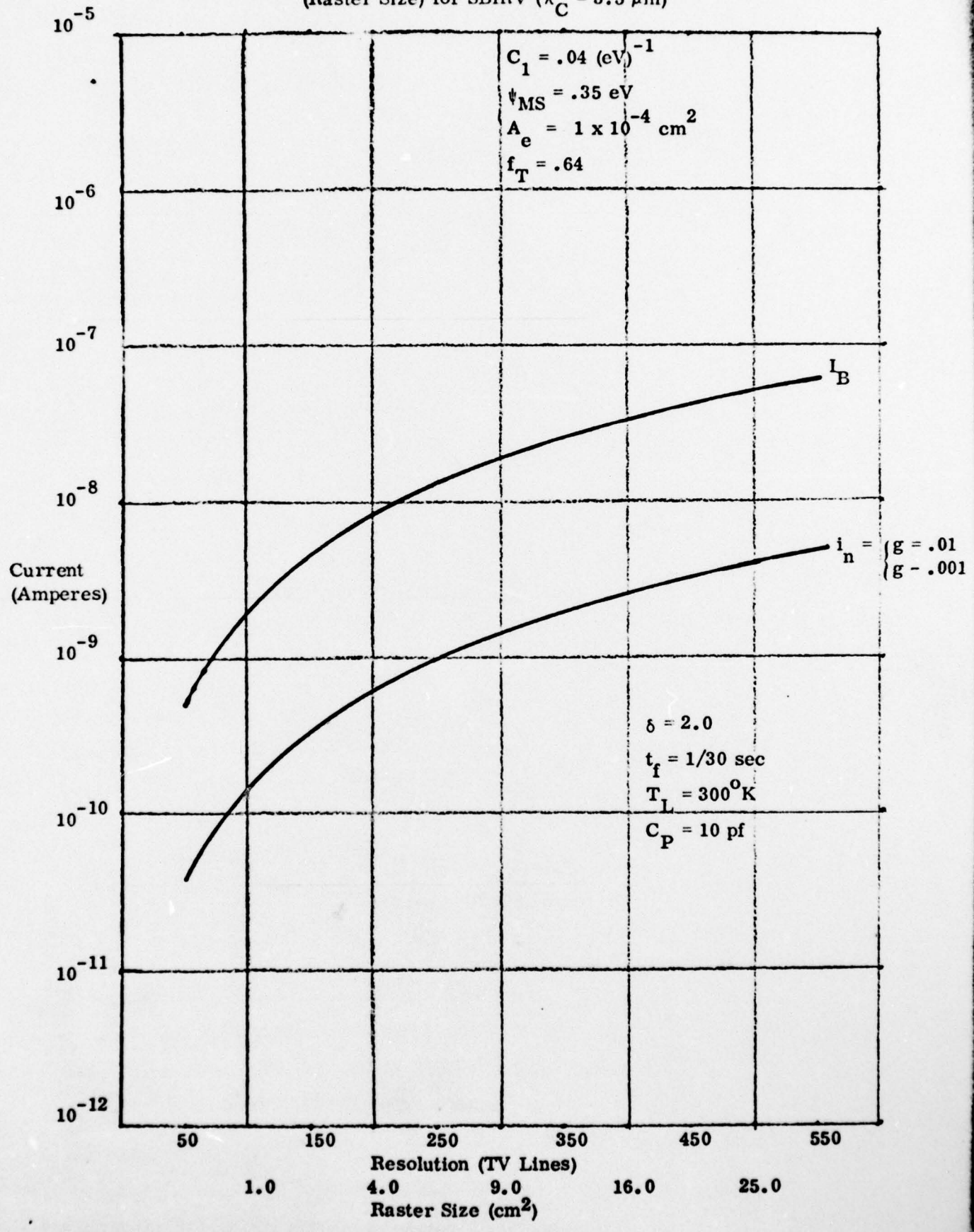

(Raster Size) for SBIRV (λ_C = 5 μm)

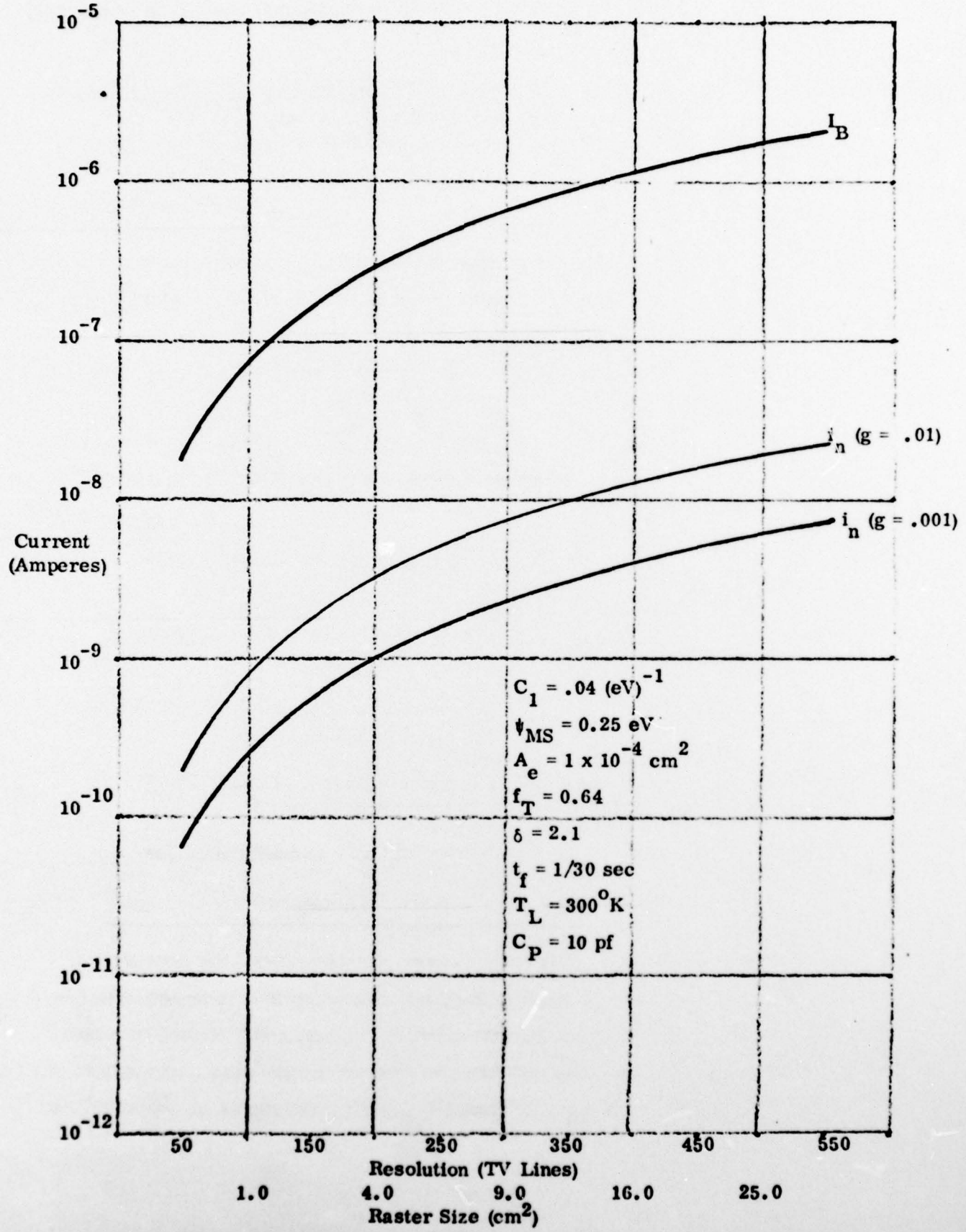

where each of these terms has now been defined. The procedure for verifying this equation is well known[15] and it consists of plotting the signal power on the retina ($P_S = H_S A_i$) necessary to produce a given signal-to-noise ratio as A_i (image area) is varied. Rewriting equation (48), it can be shown that

$$H_S A_i = \frac{(S/N)\, i_N}{R f_T A_{raster}} \left[A_i + A_e \right] \tag{49}$$

When this is plotted on log-log paper, it should produce a straight line of slope 1 for large A_i (since $\gamma = 1$), and should asymptote to

$$P_S^* = (H_S A_i)^* = \frac{(S/N)\, i_N A_e}{R f_T A_{raster}} \tag{50}$$

for $A_i \ll A_e$. The corner value of A_i is defined as A_e. Thus the following experimentally determined parameters can be defined as determined for a signal to r.m.s. noise ratio of one.

- N.E.H. (Noise Equivalent Irradiance)

$$N.E.H. = \frac{P^*}{A_e} = \frac{i_N}{R f_T A_{raster}} \tag{51}$$

- N.E.P. (Noise Equivalent Power)

$$P_e^* = N.E.P. = \frac{i_N A_e}{R f_T A_{raster}} \tag{52}$$

- Resolution Element Size, A_e

B. Experimental Results with Pd_2Si/p-Type Silicon Retinas

Pd_2Si/p-type silicon Schottky barrier diode retinas have been designed and built and have imaged successfully in the infrared. Figure 23 shows a photograph (taken from a TV monitor) of an image of a bar pattern obtained with the demountable camera tube apparatus. Quantitative imagery data was obtained from resolution element size experiments, as shown in Figure 24. Evaluating N.E.H., N.E.P. and A_e from

Figure 24. Resolution Element Size Data

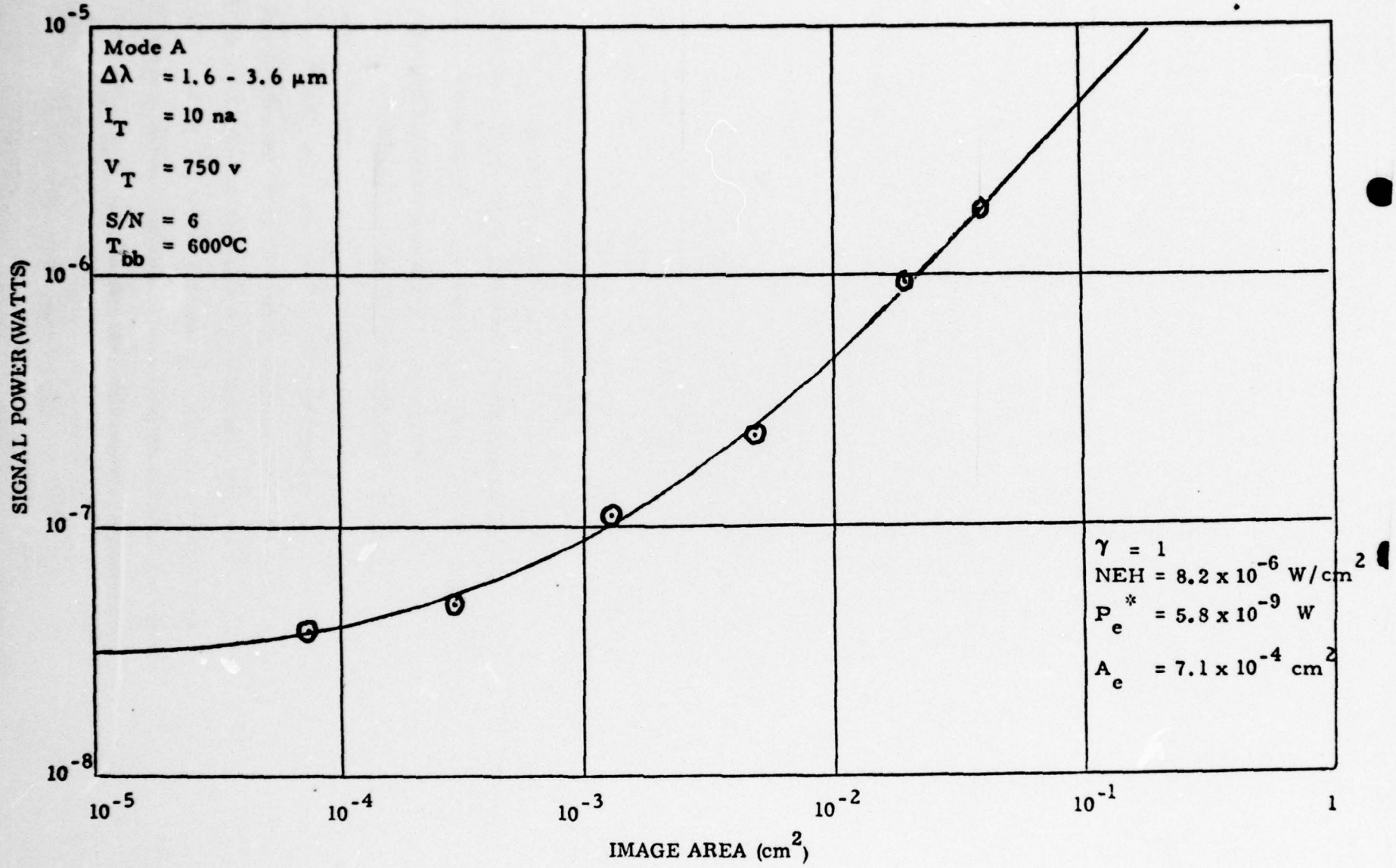

Figure 24, the following values are obtained

$$N.E.H. = 8.2 \times 10^{-6} \text{ W/cm}^2$$

$$N.E.P. = 5.8 \times 10^{-9} \text{ W}$$

$$A_e = 7.1 \times 10^{-4} \text{ cm}^2$$

These experimentally evaluated quantities permit the determination of the retina responsivity achievable in high beam velocity tubes.

1. Retina Responsivity

To assure that the resolution element size determined in these experiments was characteristic of the retina rather than the electronics, high frequency peaking was used in the video processor. The equivalent input noise current i_n measured under the conditions referenced in Figure 24 was

$$i_n = 3.8 \times 10^{-9} \text{ amperes}$$

Thus

$$R = \frac{i_n A_e}{P_e^* f_T A_{raster}} = 3.6 \times 10^{-4} \frac{\text{amps}}{\text{watt}}$$

The theoretically predicted quantum efficiency of a Pd_2Si/p-type silicon Schottky barrier detector operating against a black body at 600°C is 9×10^{-4} amperes/watt. Thus, retina responsivity determined from quantitative imagery measurements (R_I) has been found to be 0.4 of the theoretical value (Cf. Figure 17) for retina 10P115, while a determination from D.C. photoresponse ($R_{D.C.}$) gives a value 0.7 of the theoretical value for retina 14P114. It is not known at this time whether this difference is indicative of a real loss mechanism inherent in high beam velocity scanning, or of retina-to-retina variations in the constant C_1 (Cf. equation 20). If further experimentation shows it to be due to a real loss mechanism, improved retina designs (such as retinas featuring an integrated mesh) should eliminate this loss and permit full responsivity to be achieved. Otherwise, normal technology improvements expected from a maturing technology should eliminate this difference. [Note: Appendix A discusses one possible loss mechanism which would give rise to $R_I < R_{D.C.}$, and a proposed retina design to eliminate it.]

2. Resolution Element Size

The storage mode gain factor and the camera tube resolution which can be achieved in vidicon operation is determined by the ratio of the raster area, A_{raster}, to the resolution element size, A_e. The raster size is limited by the size of the retina which can be processed with good uniformity, and by the beam current available to scan it. Thus system performance is determined by how small A_e can be made. Dresner[8] has identified the physical process which will determine A_e, viz. the non-uniform redistribution of uncollected secondary electrons. Since most secondary electrons are ejected at an angle to the normal, the uncollected portion returns to the target at some distance from the point of origin. For an electron emitted with an energy V at an angle θ, the range r will be

$$r = 4d \frac{V}{eV_T} \cos\theta \sin\theta \tag{53}$$

where d = target-to-mesh spacing

V_T = voltage of target surface relative to mesh

r will maximize, for $\theta = 45^o$, at the value

$$r^* = 2d \frac{V}{eV_T} \tag{54}$$

The average energy of secondaries is $\overline{V}$, and the average target voltage V_T over a complete frame will be (Cf. equation 7)

$$eV_T = \overline{V} \ln \delta \left(1 - \frac{M}{2}\right) \tag{55}$$

where M = depth of modulation.

The resolution element size, A_e, will be determined by r^*

$$A_e = \pi r^{*2} = \pi \left[\frac{2d}{\ln \delta \left(1 - \frac{M}{2}\right)}\right]^2 \tag{56}$$

For the experiments leading to the data of Figure 24 (i.e., low background experiments),

$M \approx 0$. Thus

$$A_e\big|_{\text{low background}} = \frac{4\pi}{(\ell n\,\delta)^2}\ d^2 \tag{57}$$

[For high background experiments, $M \approx 1$, so that

$$A_e\big|_{\text{high background}} = \frac{16\pi}{(\ell n\,\delta)^2}\ d^2 \ ] \tag{58}$$

Thus a retina-to-mesh spacing of 6.5×10^{-3} cm would produce the value of A_e measured. This is in agreement with the nominal value of 5×10^{-3} cm actually used. [More precise comparison is not possible at this time since repeated temperature cyclings of the mesh used in our experiments caused wrinkling, with resultant point-to-point variations in d. This problem has since been corrected, and uniform mesh spacing over the entire retina surface can now be achieved.]

3. Summary of Experimental Results obtained in Demountable Tube

The results described above show that high beam velocity scanning can be used successfully to interrogate a matrix of internal photoemissive metal-silicon Schottky barrier diodes, and that high sensitivity infrared imaging can thereby be attained. Retina responsivity within 40% of that obtained on the best single element diodes have been measured, and no problems have been identified which would prevent full theoretical efficiency from being achieved. Resolution element size obtained to date is limited by mesh-to-retina spacing (as predicted), but new retina designs integrating the mesh directly on the retina would permit A_e to be reduced to a value limited by the diameter of the scanning beam ($A_e \approx 10^{-5}$ cm^2). In summary, the feasibility experiments have met all their objectives.

IV. PERFORMANCE EXPECTED IN INFRARED CAMERA TUBES USING SCHOTTKY BARRIER RETINAS

The foregoing discussion has shown the basic feasibility of imaging in the near to mid-infrared range with a high beam velocity camera tube employing as a retina a mosaic of metal-silicon Schottky barrier diodes operating as internal photoemissive devices. It is now possible to calculate the performance which can be expected of systems employing

such camera tubes. In preparing these estimates, two different applications will be considered, viz. the detection of very small temperature differences above (or below) background (assumed to be 300°K), and the detection of very hot objects (1000°K) at large distances. In both cases, an F/1 system will be assumed with $M \ll 1$, optic transmission $T_O = 1$, and atmospheric transmission $T_A = 1$.

A. Detection of Small Temperature Differences about Background Temperature

For this application the figure of merit for imager performance is M.R.T., defined here as the temperature of a target which will produce a signal-to-r.m.s. noise ratio of one when viewed against a background of 300°K. Expanding on equation (21) we obtain the following equation for M.R.T.

$$\frac{[R(T)H_S(T) - R(T_b)H_S(T_b)]\, f_T A_{raster}}{i_n} = 1 \qquad (59)$$

where the terms are defined in section III above. The temperature, T, which satisfies this equation is by definition the M.R.T. of the system. Table I lists the parameters needed to solve this equation for M.R.T., and the values assumed for these parameters. Values designated by an asterisk have already been achieved; those with a double asterisk are felt to be achievable with only a modest extension of existing technology. The specific steps to be taken to achieve the latter improvements include integrating the mesh directly on the retina, and increasing the size of the wafer from which the retina is fabricated to 2.5 inch diameter. (Note: The barrier height quoted for platinum silicide has been measured on single diodes. It is assumed that a platinum silicide retina will prove no more difficult to manufacture than the palladium silicide retina.) Figures 25 and 26 show the values of minimum resolvable temperature difference calculated from equation (59) as a function of limiting spatial resolution in TV lines per raster height (for a square format) for Pd_2Si retinas ($\lambda_C = 3.5\ \mu m$), and PtSi retinas ($\lambda_C = 5\ \mu m$), using the parameters of Table I. For comparison purposes, recent data[17] on the pyroelectric vidicon is also presented. These curves show that despite their comparatively short cutoff wavelength, Schottky barrier infrared vidicons are capable of quite good performance in the imaging of objects near room temperature. PtSi retinas are expected to show 0.2°C MRTD at

Table I

Parameter	Symbol	Value
1. Quantum efficiency coefficient	C_1	$.016\ eV^{-1}$ *
2. Schottky barrier height	ϕ_0	0.35 eV * (Pd_2Si) 0.25 eV * (PtSi)
3. Resolution element size (Varied by varying mesh spacing from 5×10^{-3} cm to 1×10^{-4} cm)	A_e	$7.1 \times 10^{-4}\ cm^2$ * $8 \times 10^{-5}\ cm^2$ **
4. Maximum raster area	$A_{raster\|MAX}$	$20\ cm^2$ **
5. r.m.s. spatial variation of retina responsivity (Cf. Note 1)	g	.01 * .001 **
6. Parasitic capacitance of camera tube	C_P	10 pf *
7. Temperature of retina load resistor (Cf. Note 2)	T_L	160^oK *
8. Secondary emission yield of retina	δ	2.1 *
9. Retina fill factor	f_T	0.64 *
10. Frame time	t_f	1/30 sec *

* Value already demonstrated

** Value expected with modest extension of technology

Note 1: g values < .01 have been demonstrated[14] in experiments on hard wired accessed arrays. Demonstration in a vidicon camera tube awaits the fabricating of PtSi retinas, since Pd_2Si are limited by pre-amp noise.

Note 2: R_L will be kept at retina temperature, i.e., 80^oK. Value of T_L assumed here anticipates some excess noise in electronics above the theoretical value for a resistor at 80^oK.

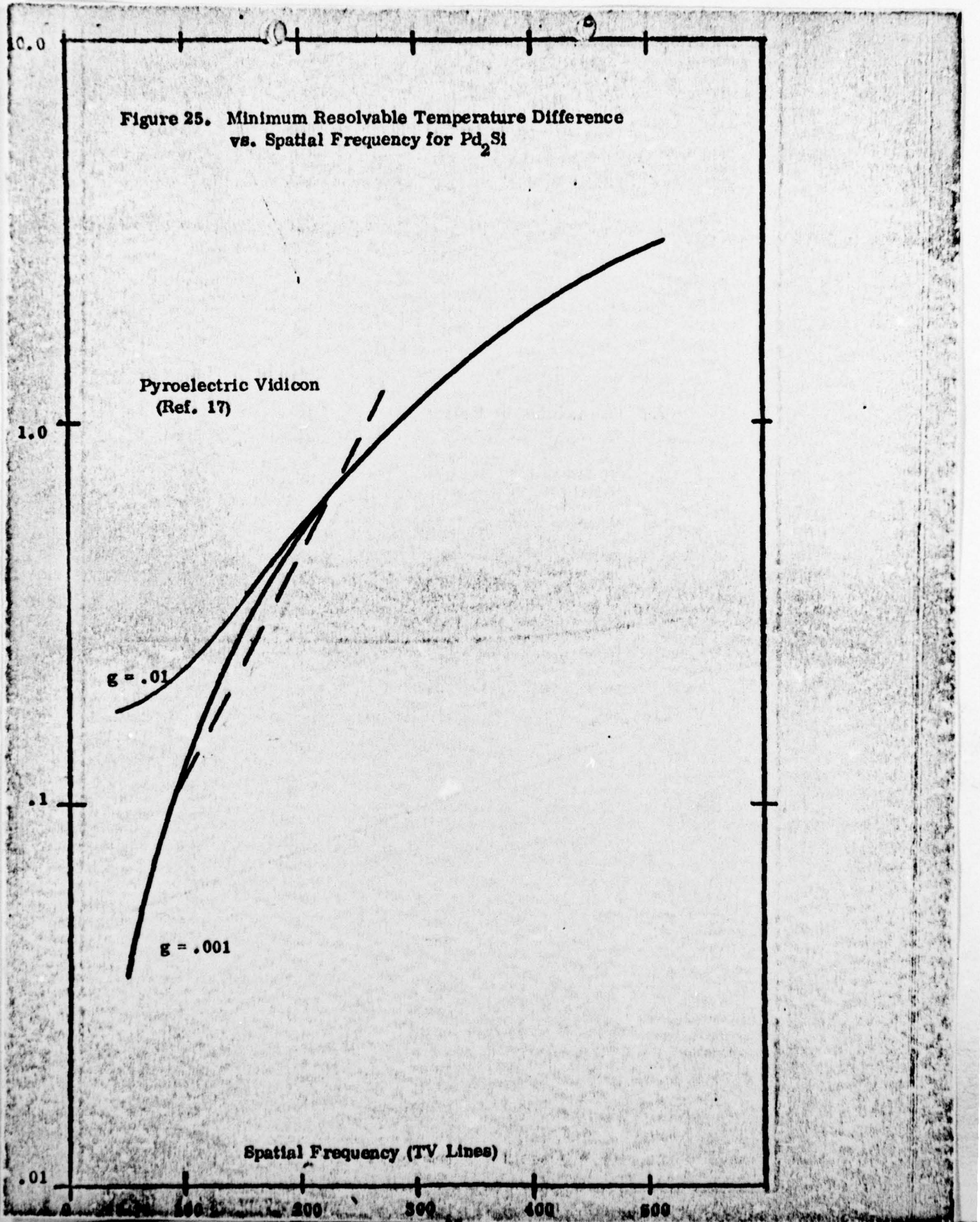

Figure 25. Minimum Resolvable Temperature Difference vs. Spatial Frequency for Pd_2Si

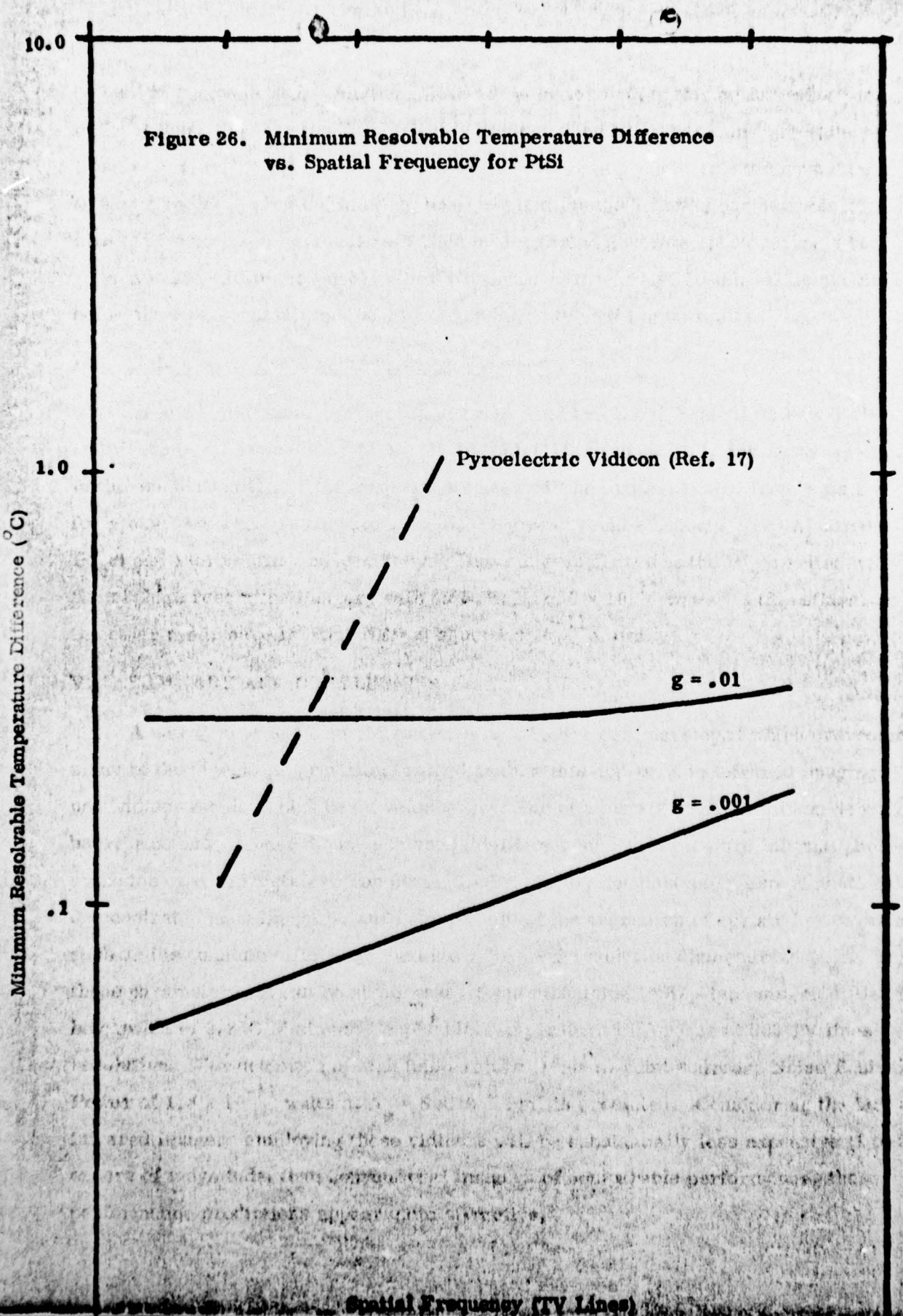

Figure 26. Minimum Resolvable Temperature Difference vs. Spatial Frequency for PtSi

500 TV lines resolution, which is substantially better than predicted for pyroelectric vidicons. Furthermore, Schottky barrier infrared vidicons maintain low values of MRTD for very low spatial frequency images, whereas pyroelectric vidicons do not. Dynamic range is also shown not to be a problem for the Schottky barrier retinas, with maximum beam currents required by background generated photocurrents being 16 na and 585 na for the Pd_2Si and PtSi retinas, respectively. (Both values are well below the 1 μa beam current usually regarded as typical for such tubes[1].)

B. Detection of Hot Objects at Large Distances

In this application, the figures of merit used are Noise Equivalent Power (P_e^*), and Resolution Element Size (A_e). P_e^* is defined by equation (52), and A_e^* by equation (58). In the calculation of P_e^*, the responsivity used will be that calculated from equation (20) for a black body temperature of 1000°K. Figures 27 and 28 show P_e^* vs. A_e for the Pd_2Si and PtSi retinas, respectively. These curves show that the Pd_2Si retina will permit high resolution imagery with an N.E.P. of 3×10^{-11} watts. PtSi retinas, on the other hand, have limiting NED at about 1×10^{-11} watts.

V. SUMMARY AND CONCLUSIONS

A new type of infrared vidicon camera tube has been developed which overcomes many of the objections previously raised against this approach to infrared imaging. This new vidicon employs high beam velocity scanning of a matrix of metal-silicon Schottky barrier diodes. These diodes achieve mid-IR response as a result of internal photoemission over the metal-silicon barrier. Feasibility demonstration experiments have demonstrated good imagery, and have permitted the evaluation of certain key parameters such as the quantum efficiency coefficient (C_1) and resolution element size (A_e). Using these parameters, it can be shown that a 5 μm tube using PtSi/p-type silicon diodes will be capable of 0.2°C Minimum Resolvable Temperature Difference at 500 TV lines resolution. For detection of high temperature (1000°K) point sources, Noise Equivalent Power of 1.3×10^{-11} watts at $A_e = 8 \times 10^{-5}$ cm^2 is predicted. Considering the fact that infrared imagers employing these vidicons will be substantially less expensive (1 to 2 orders of magnitude) than conventional imagers of comparable performance, these performance predictions appear quite attractive.

Figure 27. Noise Equivalent Power vs. Resolution Element Size for Schottky Barrier IR Vidicon (Pd_2Si/p-type Silicon)

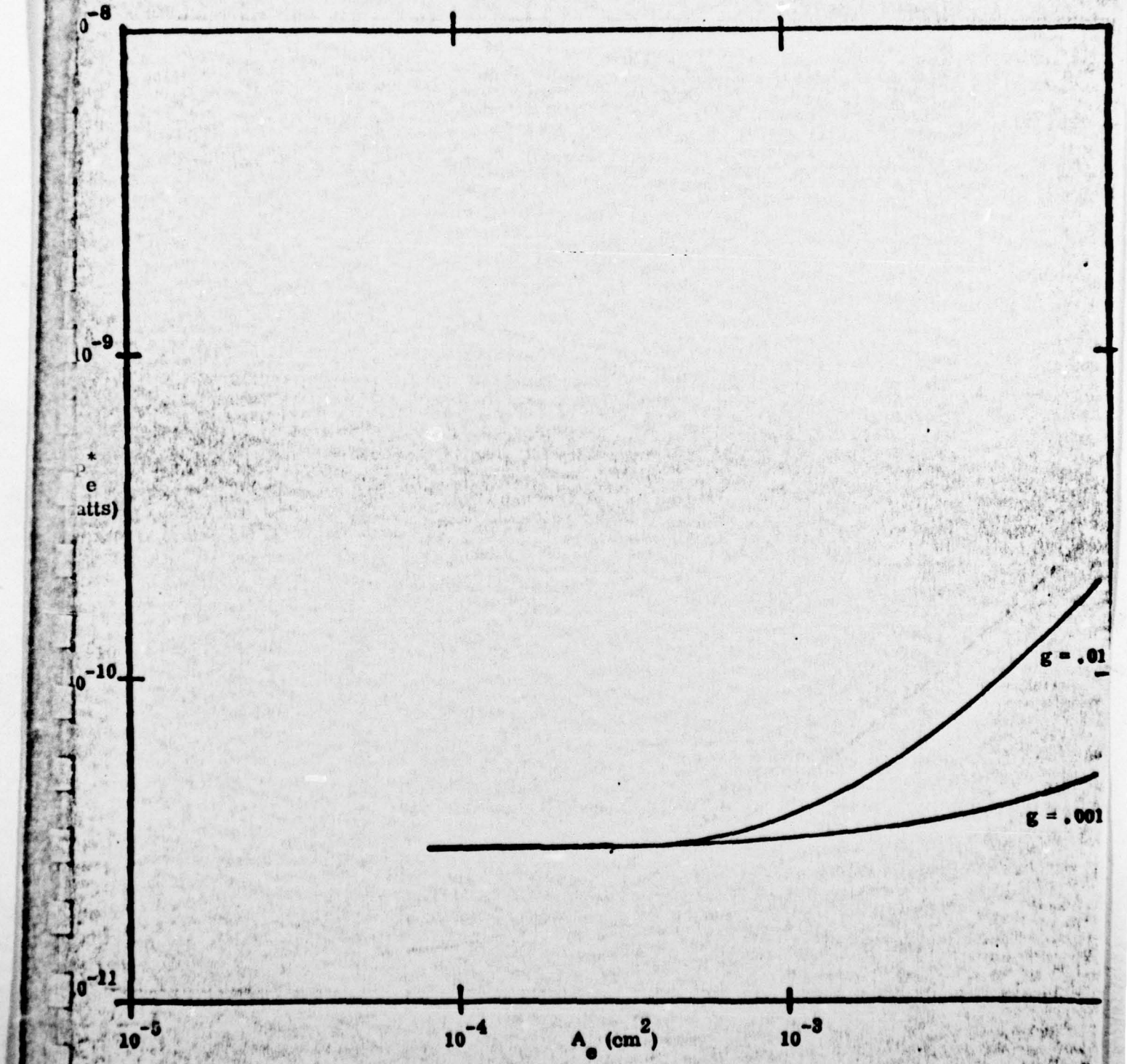

Figure 28. Noise Equivalent Power vs. Resolution Element Size for Schottky Barrier IR Vidicon (PtSi/p-type Silicon)

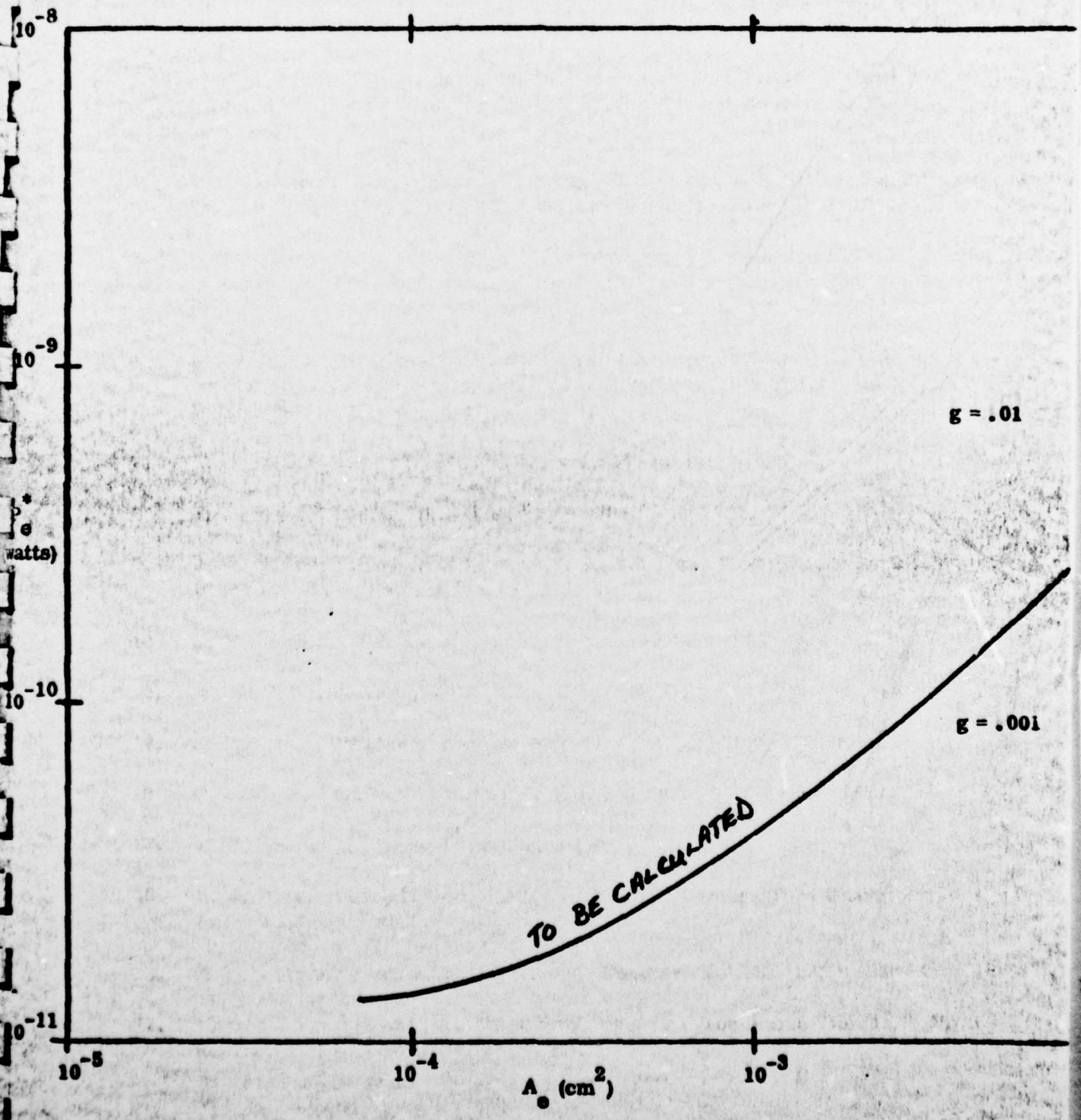

REFERENCES

1. J. A. Hall, Applied Optics, Vol. 10, pp. 838-844, (1971).

2. J. O. Dimmock, Lincoln Lab Tech Note ESD-TR-71-318, (1971).

3. J. P. Spratt and R. F. Schwarz, "Metal-Silicon Schottky Diode Arrays as Infrared Vidicon Retinas," Proc. International Electron Devices Meeting, Dec. 1973.

4. F. D. Shepherd, Jr., and A. C. Yang, "Silicon Schottky Retinas for Infrared Imaging," Proc. International Electron Devices Meeting, Dec. 1973.

5. F. D. Shepherd, et al., "Silicon Schottky Barrier Monolithic IRTV Focal Planes," in Sequin and Tompsett, "Charge Transfer Devices," Supplement 8 to Advances in Electronics & Electron Physics, Academic Press, 1975.

6. R. Williams, "Injection by Internal Photoemission," Chapter 2, Vol. 6, Semiconductors and Semimetals, Ed. by R. K. Willardson and A.C. Beer, Academic Press, (1970).

7. M. H. Crowell, et al., B.S.T.J., Vol. 46, p. 491, (1965).

8. J. Dresner, RCA Review, Vol. 22, p. 305, June 1961.

9. J. P. Spratt, G. W. Racette, and T. J. Maresca, "Facility for Evaluating Infrared Vidicon Retinas," to be published.

10. A. S. Jensen, RCA Review, Vol. 16, p. 216, June 1955.

11. V. L. Dalal, J.A.P., Vol. 42, p. 2280, (1971).

12. S. M. Sze, "Physics of Semiconductor Devices," Wiley, (1969).

13. R. Kollath, Handbuck der Physik, Vol. 21, Springer (Berlin), 1956.

14. F. D. Shepherd, private communication.

15. P. J. Daly, et al., "Determination of Infrared Camera Tube Characteristics," Proc. IRIS, Jan. 1965.

16. S. V. Forgue, et al., Trans. Electron Devices, Vol. ED-22, p. 904, Oct. 1975.

17. T. Conklin and B. Singer, "High Performance Pyroelectric Vidicon," Proc. International Electron Devices Meeting, Dec. 1975.